COMPUTATIONS OF UNSTEADY TRANSONIC FLOW GOVERNED BY THE CONSERVATIVE FULL POTENTIAL EQUATION USING AN ALTERNATING DIRECTION IMPLICIT ALGORITHM

PETER M. GOORJIAN
INFORMATICS INC.
1121 SAN ANTONIO ROAD
PALO ALTO, CALIFORNIA 94303

JUNE 1979

PREPARED UNDER CONTRACT NO. NAS2-9891

FOR

AMES RESEARCH CENTER
NATIONAL AERONAUTICS AND SPACE ADMINISTRATION

COMPUTATIONS OF UNSTEADY TRANSONIC FLOW GOVERNED BY THE CONSERVATIVE FULL POTENTIAL EQUATION USING AN ALTERNATING DIRECTION IMPLICIT ALGORITHM

Peter M. Goorjian

Informatics Inc.
1121 San Antonio Road
Palo Alto, California 94303

SUMMARY

An alternating direction implicit algorithm is presented for solving the conservative, full potential equation for unsteady, transonic flow. A new development is the time linearization of the density function. This linearization reduces the solution process from solving a system of two equations at each mesh point to solving just a single equation. Two sample cases are computed. First, a one dimensional traveling shock wave is computed and compared with the analytic solution. Second, a two dimensional case is computed of a flow field which results from a thickening and subsequently thinning airfoil. The resulting flow field, which includes a traveling shock wave, is compared to the flow field obtained from the low frequency, small disturbance, transonic equation.

TABLE OF SYMBOLS

a	speed of sound
c	characteristic length, e.g. chord length
d	characteristic time
$k = \omega c/q_\infty$	reduced frequency
$M = q/a$	Mach number
p	pressure
C_p	pressure coefficient
$\vec{q}$, q	velocity, speed
t, τ	time
u	x component of velocity
v	y component of velocity
γ	specific heat ratio
ϕ	velocity potential
ρ	density
ω	circular frequency
$\vec{\nabla} = (\partial_x, \partial_y)$	gradient operator
$[Q] = Q_+ - Q_-$	jump or difference in the quantity Q on the two sides of a surface of discontinuity

Subscript

∞	indicator of free stream values, e.g. M_∞ denotes free stream Mach number

I. INTRODUCTION

Unsteady transonic flows are one of the most important yet least understood areas in fluid mechanics.[1] For example, dips in flutter boundaries are often observed in the transonic Mach number range.[2-3] An especially pronounced dip was observed for a supercritical wing.[4] However, the mechanism for this dip is not yet understood. Other important problems in unsteady transonic flows are the flow about helicopter rotor blades,[5] gust alleviation at transonic speeds, active control for dynamic stability at transonic speeds and transonic flow in turbines.

This work is intended to provide a computational tool for the study of unsteady transonic flow and especially for the prediction of unsteady loads on aerodynamic bodies. We present an algorithm which solves the two dimensional conservative, full potential equation for unsteady flow. This equation will properly account for nonlinear effects, such as moving shock waves, under the assumptions that the viscous and rotational aspects of the flow are negligible. However it may be possible in the future to take into account those aspects in the case of a shock wave boundary layer interaction by coupling this algorithm with an unsteady boundary layer algorithm.

This algorithm uses methods similar to those used to solve the low frequency, small disturbance equation.[6-8] As in that earlier development, certain criteria were used in choosing the methods.

First, the algorithm should have fast computer run times, so that it can be routinely used for engineering applications. Hence the choice was made to develop a finite difference, alternating direction implicit algorithm. Such implicit algorithms permit large time steps; consequently the consideration of step size is based more on accuracy than on stability.

Second, the algorithm should properly treat unsteady nonlinear effects, including moving shock waves. Presently, there is no well established method of shock fitting for unsteady flow. However, shock capturing methods are in common use.[7,9] Therefore we choose the method of solving the governing equation in conservation form to ensure that the captured shock speed is the theoretically correct one. Calculations[6,10] based on equations in nonconservative form can produce captured shock speeds which depend on nonphysical parameters, such as mesh spacing or time step size.

Third, the algorithm should properly handle aerodynamic shapes, arbitrary motions of those shapes, and arbitrary free stream Mach numbers. We choose the full potential equation as the governing equation. This equation removes three limitations[6-7,11] on this third criterion which are assumed by low frequency, small disturbance, transonic, potential theory. These limitations are (1) that the flow field can be represented as a small perturbation about the free stream velocity, (2) that only low frequencies occur in the motion of the fluid and (3) that the free stream Mach number is close to one. This removal is especially necessary for the

accurate flutter analysis of supercritical airfoils. Such airfoils are thick and blunt nosed, and full potential theory properly handles these features.

The fourth criterion considered was that the algorithm should be extendible to the three space dimensions. Alternating direction implicit methods are generally extendible.[6,12-13]

Hence by the use of these criteria, we have decided to solve the unsteady, conservative, full potential equation by an alternating direction implicit method. This equation has two variables, viz. density and potential. So for a well posed problem we must augment the full potential equation with the unsteady Bernoulli equation to form a system of two equations.

A new algorithm development is reported in this paper which simplifies the solution process for the resulting system of two finite difference equations at each mesh point. This development is the linearization backward in time of the nonlinear density function in the full potential equation. The linearization uses the unsteady Bernoulli equation and reduces the solution process to one which requires only the solution of a single equation at each mesh point for the potential.

In Section II the assumptions made in deriving the governing equations are stated and those equations are presented in a general curvilinear coordinate system. In Section III the algorithm is tested on a one dimensional traveling shock wave, for which the analytic solution is known. In Section IV a two dimensional flow is computed. Here a thickening and subsequently thinning airfoil produces a flow field with a rich structure, including a shock wave that travels in a large excursion. The computed results are found to be in close agreement with computed results from low frequency, small disturbance, transonic theory, as expected for this special case.

II. FORMULATION OF THE GOVERNING EQUATIONS

The following assumptions are made on the flow of a perfect gas and the resulting nondimensionalized governing equations are given.

1. Mass is conserved.

$$k \frac{\partial \rho}{\partial t} + \vec{\nabla} \cdot \rho \vec{q} = 0 \ . \tag{1}$$

2. The flow is irrotational.

$$\vec{q} = \vec{\nabla} \phi \ . \tag{2}$$

3. The flow is isentropic.

$$p = \frac{1}{\gamma M_\infty^2} \rho^\gamma \quad , \quad a^2 = \frac{\gamma p}{\rho} \tag{3}$$

4. The flow is inviscid.

From assumptions 2, 3 and 4, the momentum equation can be integrated[14] to yield the unsteady Bernoulli equation.

$$k \frac{\partial \phi}{\partial t} + \frac{1}{2} q^2 + \frac{a^2}{\gamma - 1} = \frac{1}{2} + \frac{1}{M_\infty^2 (\gamma - 1)} \ . \tag{4}$$

Here the constant of integration is chosen so that for steady flow, Eq. (4) reduces to the steady Bernoulli equation. The variables have been nondimensionalized in cartesian coordinates (t, x, y) as follows: x by c, y by c, t by d, ϕ by $q_\infty c$, a by q_∞, ρ by ρ_∞ and p by $\rho_\infty q_\infty^2$. If there is a characteristic frequency ω in the problem, then $d = 1/\omega$ and k is the reduced frequency;

$$k = \omega c / q_\infty \ . \tag{5}$$

Otherwise, $k = 1$, $d = c/q_\infty$ and time is measured in characteristic lengths travelled at free stream speed q_∞. Here c is a characteristic length, which we choose as the chord length of the airfoil.

Eq. (1) is in conservation form and hence has weak solutions,[15] which conserve mass across surfaces where the flow variables are discontinuous. The jump condition, which is built into Eq. (1), is given by

$$[k\rho] \frac{\partial S}{\partial t} + [\rho u] \frac{\partial S}{\partial x} + [\rho v] \frac{\partial S}{\partial y} = 0 \ , \tag{6}$$

where the surface of discontinuity is given by $S(x,y,t) = 0$, and $[\ ]$ denotes the difference of the enclosed quantity on opposite sides of S.

Computations of solutions to the flow equations about aerodynamic bodies are made more efficient by the use of a coordinate system that is adapted to the shape of the body and its motion. Hence we wish to write the flow equations, Eqs. (1) and (4) in a general coordinate system. Let (τ,ξ,η) be related to cartesian coordinates (t,x,y) by the transformation

$$\xi = \xi\ (x,y,t), \quad \eta = \eta\ (x,y,t), \quad \tau = t\ . \tag{7}$$

Then the conservation of mass equation in covariant form is given by

$$k\ \frac{\partial}{\partial\tau}\left(\frac{\rho}{|J|}\right) + \frac{\partial}{\partial\xi}\left(\frac{\rho U}{|J|}\right) + \frac{\partial}{\partial\eta}\left(\frac{\rho V}{|J|}\right) = 0\ . \tag{8}$$

See Appendix A for the derivation of Eq. (8). $|J|$ is the absolute value of the Jacobian of the transformation (7), where

$$J = \xi_x\eta_y - \xi_y\eta_x\ . \tag{9}$$

U and V are the contravariant components of the velocity $\vec{q}$ in the ξ and η directions respectively, where

$$\begin{aligned} U &= \xi_t + \xi_x u + \xi_y v\ , \\ V &= \eta_t + \eta_x u + \eta_y v\ , \end{aligned} \tag{10}$$

and $\vec{q} = (u,v)$ in Cartesian coordinates. From Eq. (2), $\vec{q} = (\phi_x, \phi_y)$, hence by the chain rule for differentiation,

$$\begin{aligned} U &= \xi_t + A_1\phi_\xi + A_2\phi_\eta\ , \\ V &= \eta_t + A_2\phi_\xi + A_3\phi_\eta\ , \end{aligned} \tag{11}$$

where,

$$\begin{aligned} A_1 &= \xi_x^2 + \xi_y^2\ , \\ A_2 &= \xi_x\eta_x + \xi_y\eta_y\ , \\ A_3 &= \eta_x^2 + \eta_y^2\ . \end{aligned} \tag{12}$$

Using Eqs. (3) and (4) and $q^2 = \phi_x^2 + \phi_y^2$, one obtains

$$\rho = \left[1 + M_\infty^2 \frac{(\gamma-1)}{2} \left\{ 1 - 2\phi_\tau - (\xi_t + U)\phi_\xi - (\eta_t + V)\phi_\eta \right\}\right]^{\frac{1}{\gamma-1}} . \quad (13)$$

Equations (8) and (13) form the system of equations which will be solved in the domain of the variables (τ,ξ,η).

To complete the formulation of the problem, we specify the boundary and initial conditions. For inviscid flow, the boundary condition on an aerodynamic body is given by the physical requirement that the motion of the fluid is tangent to the body as the body moves. We will describe the body by

$$\eta\ (x,y,t) = 0 . \quad (14)$$

Mathematically, this boundary condition is that the physical component[16] of the velocity along $\eta = 0$ is zero; this condition is equivalent to

$$V = 0 . \quad (15)$$

In the sample computation of a two-dimensional nonlifting flow presented in this report, the far field boundary condition is that the flow variables have their steady free stream values. The initial conditions are obtained from the steady flow field, which is assumed to exist for $t \leq 0$.

Note that in a general flow problem, one can use an η equals constant surface to describe the location of an outer boundary. An example is flow in a wind tunnel, where an η -equals-constant surface locates a wall. Another advantage of using a general coordinate system is the ability to cluster mesh points[17] in regions of interest, such as shock waves or stagnation points, without disrupting the smoothness of the mesh.

The two dimensional calculations will be studied by plotting the resulting pressure coefficients, Cp, versus position on the airfoil. The formula for Cp is

$$Cp = \frac{2}{\gamma M_\infty^2} (\rho^\gamma - 1) . \quad (16)$$

Recall, before nondimensionalization $Cp = (p - p_\infty)/Q$, where $Q = (1/2)\ \rho_\infty q_\infty^2$ is the free stream dynamic pressure.

III. ONE DIMENSIONAL SHOCK WAVE MOTION

First, we will compute the one dimensional case of a travelling shock wave. The shock wave travels downstream and separates supersonic flow upstream from subsonic flow. Here the state of the fluid is measured relative to the coordinate system and not relative to the moving shock. The exact analytic solution is known, so by comparison with the computed results, the shock capturing properties of the algorithm can be examined. In particular, we can verify that the algorithm is computing the correct shock speed, which is given by the jump condition, Eq. (6).

a) Model Problem

For this problem, we use cartesian coordinates, (x,t). Equations (8) and (13) simplify to

$$\rho_t + (\rho\phi_x)_x = 0 \quad , \tag{17a}$$

$$\rho = \left[1 + M_\infty^2 \left(\frac{\gamma-1}{2}\right)\left(1 - 2\phi_t - \phi_x^2\right)\right]^{\frac{1}{\gamma-1}} \tag{17b}$$

The flow is along a finite interval and the length, L, of the interval is used for the characteristic length. Also, k = 1. The initial and boundary conditions are

$$\phi\ (0,t) = 0, \quad \phi_x\ (0,t) = U_L = 1, \quad \phi_x\ (1,t) = U_R = 0.8,$$

$$\phi\ (x,0) = \begin{cases} x & , \quad 0 \le x \le xs_o\ , \\ xs_o + (x - xs_o)\ U_R, & \quad xs_o \le x \le 1, \end{cases} \tag{18}$$

$xs_o = 0.045$ and is the initial position of the shock.

Here the velocity is nondimensionalized by the upstream (i.e., left side) velocity; Figure 1 shows the initial conditions.

The solution to Eqs. (17) and (18) is

$$\phi\ (0,t) = 0$$

$$\phi_x\ (x,t) = \begin{cases} u_L & , \quad 0 \le x \le xs\ (t), \\ u_R & , \quad xs\ (t) \le X \le 1, \end{cases} \tag{19a}$$

$$xs\ (t) = xs_o + V_s \cdot t, \quad t \ge 0, \tag{19b}$$

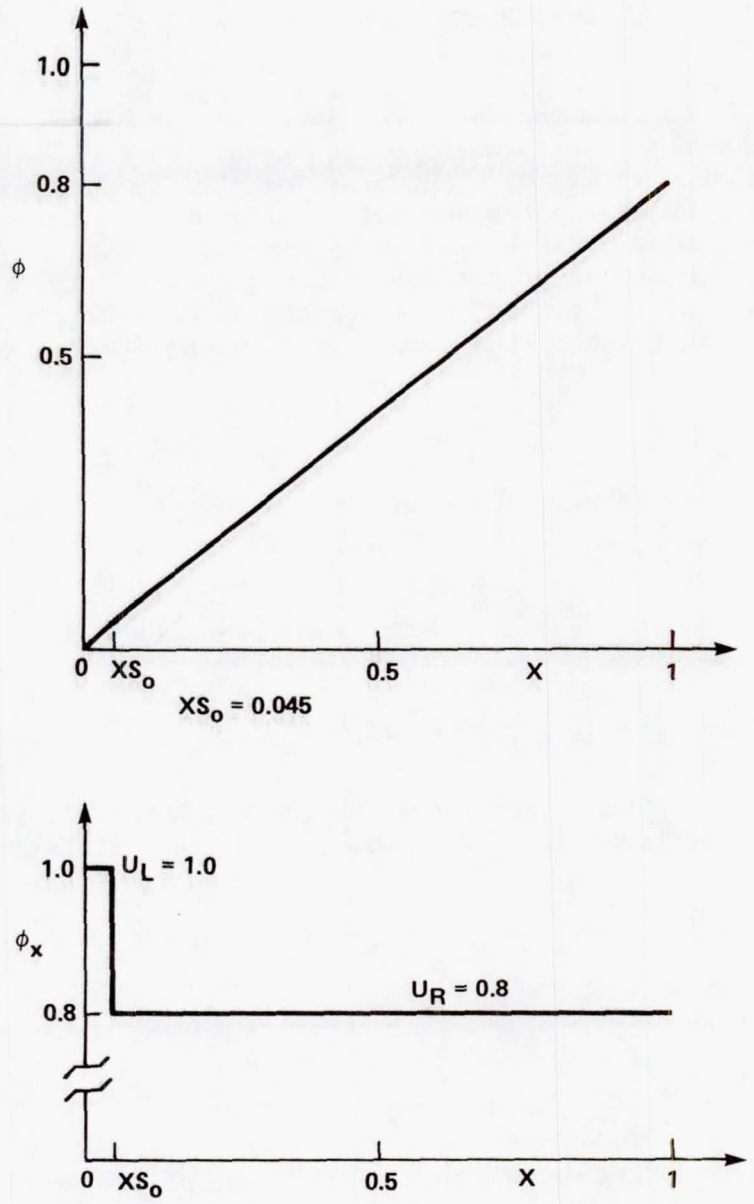

Figure 1.— Initial Conditions for One Dimensional Problem.

where $xs(t)$ is the shock location at time t and V_s is the shock velocity. V_s is determined by the shock jump condition, Eq. (6), which for this case becomes

$$(\rho_R - \rho_L)\, V_s = \rho_R u_R - \rho_L u_L, \tag{20}$$

where ρ_L and ρ_R are the upstream and downstream values of ρ. Using Eq. (17b) for ρ_L and ρ_R in Eq. (20), we see that V_s is determined by the parameters, M_∞, u_L, u_R, $(\phi_t)_L$ and $(\phi_t)_R$, where $(\phi_t)_L$ and $(\phi_t)_R$

are the upstream and downstream values of ϕ_t. In our nondimensionalization of the variables in this one dimensional problem, we normalize by upstream values, so that $u_L = 1$ and $\rho_L = 1$. From Eq. (17b), it follows that $(\phi_t)_L = 0$.

In smooth regions of space time (x,t), the potential function $\phi(x,t)$ satisfies

$$\phi_{xt} = \phi_{tx} \ . \tag{21}$$

At a discontinuity, the shock jump condition which follows from Eq. (21) is

$$[\phi_x] \frac{\partial S}{\partial t} = [\phi_t] \frac{\partial S}{\partial x} \ , \tag{22}$$

where $S(x,t) = 0$ is the curve of discontinuity in (x,t). Since

$$V_s \frac{\partial S}{\partial x} + \frac{\partial S}{\partial t} = 0 \ , \tag{23}$$

$u_L = 1$ and $(\phi_t)_L = 0$, we have

$$(\phi_t)_R + V_s \ (u_R - 1) = 0. \tag{24}$$

Using Eq. (24) in Eq. (17b),

$$\rho_R = \left[1 + M_\infty^2 \left(\frac{\gamma-1}{2} \right) \left\{ 1 - (u_R)^2 - 2V_s(1 - u_R) \right\} \right]^{\frac{1}{\gamma-1}} \tag{25}$$

Using Eq. (25) in Eq. (20), we obtain a transcendental equation for V_s as a function of M_∞ and u_R. Since $\rho_L = u_L = 1$, Eq. (20) simplifies to

$$(\rho_R - 1) \ V_s = \rho_R u_R - 1 \ . \tag{26}$$

The following iterative scheme was used to determine V_s for the sample case computed, for which $M_\infty = 1.2$ and $u_R = 0.8$. First, an initial guess of V_s was made. Next, Eq. (25) was used to compute ρ_R. Then Eq. (26) was used to compute a new value of V_s. By a few choices of the initial guess for V_s, one was found which would generate a convergent sequence for V_s by iteration, using Eqs. (23) and (24) as described. The resultant V_s used was $V_s = 0.4474296609271$. This value of V_s is used in Eqs. (19) to complete the description of the analytic solution.

b) 1-D Algorithm

Next we present the algorithm used to compute this flow. First order accurate in time, implicit Euler, finite difference approximations to Eqs. (17) at the mesh point (i,n), located at the point $(x,t) = (i\Delta x, n\Delta t)$ in the flow domain are

$$\overleftarrow{\delta}_t \rho_i^{n+1} + \overleftarrow{\delta}_x \left(\rho_{i+1/2}^{n+1} \overrightarrow{\delta}_x \phi_i^{n+1} \right) = 0 \quad , \tag{27a}$$

$$\rho_i^{n+1} = \left[1 + M_\infty^2 \left(\frac{\gamma-1}{2} \right) \left\{ 1 - 2\overleftarrow{\delta}_t \phi_i^{n+1} - \left(\delta_x \phi_i^{n+1} \right)^2 \right\} \right]^{\frac{1}{\gamma-1}} , \tag{27b}$$

$$\rho_{i+1/2}^{n+1} = \frac{1}{2} \left(\rho_{i+1}^{n+1} + \rho_i^{n+1} \right) , \tag{27c}$$

where

$$\overleftarrow{\delta}_t = (\Delta t)^{-1} \left(1 - E_t^{-1} \right) , \quad 0 \, (\Delta t)$$

$$\overleftarrow{\delta}_x = (\Delta x)^{-1} \left(1 - E_x^{-1} \right) , \quad 0 \, (\Delta x)$$

$$\overrightarrow{\delta}_x = (\Delta x)^{-1} \left(E_x^{+1} - 1 \right) , \quad 0 \, (\Delta x)$$

$$\delta_x = (2\Delta x)^{-1} \left(E_x^{+1} - E_x^{-1} \right) , \quad 0 \, (\Delta x^2) \, .$$

The shift operators are defined by

$$E_t^{\pm 1} \phi_i^n = \phi_i^{n \pm 1} \quad ,$$

$$E_x^{\pm 1} \phi_i^n = \phi_{i \pm 1}^n \quad .$$

Eqs. (27) form a system of two implicit equations at each mesh point (i, n + 1) for the dependent variables ρ_i^{n+1} and ϕ_i^{n+1}. A key idea developed in this report is the approximation of Eq. (27a) by an equation in which only the unknowns ϕ_i^{n+1} occur and they occur in a linear manner. The technique used for this approximation is the time linearization procedure commonly used for the analysis and numerical solution of nonlinear differential equations.[10] Although it is common practice[6,10] to time linearize the nonlinear functions occurring in the space differences, here we will time linearize the nonlinear function occurring in the time difference in Eq. (27a) as well, by use of the special algebraic structure that the density possesses in Eq. (27b)(see acknowledgement). The resulting equation will preserve the property of conservation form, which is possessed by Eq. (27a).

First we will time linearize the nonlinear function in the space difference in Eq. (27a) by the following substitution for the density.

$$\rho_{i+1/2}^{n+1} = \rho_{i+1/2}^{n} + 0\,(\Delta t)\ . \tag{28}$$

Next we will time linearize the nonlinear function in the time difference in Eq. (27a) by the following Taylor series expansion for ρ_i^{n+1}. We have

$$\rho_i^{n+1} = \rho_i^n + \left(\frac{\partial \rho}{\partial t}\right)_i^n \Delta t + 0\,(\Delta t^2)\ .$$

Using Eq. (27b) for ρ_i^n, we calculate $(\partial\rho/\partial t)_i^n$ and substitute into the previous equation to obtain

$$\rho_i^{n+1} = \rho_i^n - \Delta t M_\infty^2 \left(\rho_i^n\right)^{2-\gamma}\left[\overleftarrow{\delta}_t\left(\overleftarrow{\delta}_t \phi_i^{n+1}\right) + \left\{\delta_x \phi_i^n\right\}\left\{\overleftarrow{\delta}_t\left(\delta_x \phi_i^{n+1}\right)\right\}\right] + 0\,(\Delta t^2)\ . \tag{29}$$

Substitution of Eqs. (28) and (29) into Eq. (27a) yields the first order accurate in time equation

$$\overleftarrow{\delta}_t\left\{\rho_i^n - \Delta t M_\infty^2 \left(\rho_i^n\right)^{2-\gamma}\left[\overleftarrow{\delta}_t\left(\overleftarrow{\delta}_t \phi_i^{n+1}\right) + \left\{\delta_x \phi_i^n\right\}\left\{\overleftarrow{\delta}_t\left(\delta_x \phi_i^{n+1}\right)\right\}\right]\right\} + \overleftarrow{\delta}_x\left(\rho_{i+1/2}^n \overrightarrow{\delta}_x \phi_i^{n+1}\right) = 0\ . \tag{30}$$

Note Eq. (30) is in conservation form, ϕ_i occur at level $n+1$ in a linear manner and ρ_i do not occur at level $n+1$.

Using Eq. (27b) to determine ρ_i^n, we now proceed to solve the scalar Eq. (30) at each mesh point. By algebraic operations, Eq. (30) is converted to the form

$$\phi_i^{n+1} + \tilde{A}\,\delta_x \phi_i^{n+1} + B\,\overleftarrow{\delta}_x\left(\rho_{i+1/2}^n \overrightarrow{\delta}_x \phi_i^{n+1}\right) = \tilde{C} \tag{31}$$

where

$$\tilde{A} = \Delta t\ \delta_x \phi_i^n$$

$$B = -\Delta t^2 / M_\infty^2 \left(\rho_i^n\right)^{2-\gamma}$$

$$\tilde{C} = 2\phi_i^n - \phi_i^{n-1} + \Delta t\left(\delta_x \phi_i^n\right)^2 + \left(\Delta t^2 / M_\infty^2 \left(\rho_i^n\right)^{2-\gamma}\right)\tilde{D}\ ,$$

$$\tilde{D} = \overleftarrow{\delta}_t \rho_i^n + M_\infty^2 \left(\rho_i^{n-1}\right)^{2-\gamma}\left[\overleftarrow{\delta}_t\left(\overleftarrow{\delta}_t \phi_i^n\right) + \left\{\delta_x \phi_i^{n-1}\right\}\left\{\overleftarrow{\delta}_t\left(\delta_x \phi_i^n\right)\right\}\right]\ .$$

Next we discuss our method of adding artificial dissipation. Numerical experiments indicate that Eq. (32) is a stable finite difference scheme

for subsonic regions of flow. In supersonic regions we shall add an artificial dissipation term in order to damp numerical instabilities.[18] The manner in which we add dissipation is to retard the evaluation of the density[17,19-20] in the upwind direction, for the density term which occurs in the space difference. Hence in Eq. (31), $\rho^n_{i+1/2}$ is replaced by $\tilde{\rho}^n_{i+1/2}$, an upwinded evaluation given by

$$\tilde{\rho}^{\,n}_{i+1/2} = \left(1 - \nu^n_i\right) \rho^n_{i+1/2} + \nu^n_i \rho^{\,n}_{i-1/2} \,. \tag{32}$$

The upwind weighting factor ν^n_i strongly affects the stability and accuracy of the computation. Insufficiently large values of ν^n_i can result in overshoots at shock waves or even unstable calculations. Too large values of ν^n_i result in solutions in which the shock profile is greatly smeared. Experience has shown that for unsteady flows, the proper values for ν^n_i depend on the computational mesh, the time step, the shock speed, and the shock strength. Currently the procedure for choosing ν^n_i is trial and error. In this example,

$$\nu^n_i = \min\left[1,\ \max\left\{0, \left(\left(M^n_i\right)^2 - 1\right) c\right\}\right] \,, \tag{33}$$

where c is a positive constant, which for the case shown was tuned to 7.5 and M^n_i is the local Mach number,

$$\left(M^{\,n}_i\right)^2 = \left(\delta_x \phi^n_i\right)^2 / \left(a^n_i\right)^2 \,. \tag{34}$$

Using Eq. (4), one obtains

$$\left(a^n_i\right)^2 = \frac{1}{M^2_\infty} + \left(\frac{\gamma-1}{2}\right)\left(1 - 2\overleftarrow{\delta}_t \phi^n_i - \left(\delta_x \phi^n_i\right)^2\right) \,. \tag{35}$$

In Eq. (33) the purpose of the min function is to retain an interpolation form in Eq. (32); otherwise unstable calculations can occur. For example, in the case presented here, removal of the min restriction caused the calculation to become unstable.

Also, guided by the differencing of the low frequency, small disturbance, transonic equation[6-7], certain $\delta_x \phi_i$ terms were replaced by $\overleftarrow{\delta}_x \phi_i$ terms in order to enhance the stability properties of the method. The final algorithm is given by

$$\phi^{n+1}_i + A\,\overleftarrow{\delta}_x \phi^{n+1}_i + B\,\overleftarrow{\delta}_x \left(\tilde{\rho}^n_{i+1/2}\,\overrightarrow{\delta}_x \phi^{n+1}_i\right) = C, \tag{36}$$

where

$$A = \Delta t \overleftarrow{\delta}_x \phi_i^n \quad ,$$

$$C = 2\phi_i^n - \phi_i^{n-1} + \Delta t \left(\overleftarrow{\delta}_x \phi_i^n\right)^2 + \left(\Delta t^2 / M_\infty^2 \left(\rho_i^n\right)^{2-\gamma}\right) D \quad ,$$

$$D = \overleftarrow{\delta}_t \rho_i^n + M_\infty^2 \left(\rho_i^{n-1}\right)^{2-\gamma} \left[\overleftarrow{\delta}_t \left(\overleftarrow{\delta}_t \phi_i^n\right) + \left\{\overleftarrow{\delta}_x \phi_i^{n-1}\right\}\left\{\overleftarrow{\delta}_t \left(\overleftarrow{\delta}_x \phi_i^n\right)\right\}\right] \quad .$$

c) Calculated Results

The results of a calculation of the model problem are compared with the analytic solution in Figure 2. For the calculations, 101 equally spaced mesh points were used on the unit interval in the x direction. Also, since the velocity of the shock is known, the time step, Δt, was chosen so that the shock moves one-half mesh space per time step. The shock was initially located half-way between mesh points $i = 5$ and $i = 6$; $xs(0) = 0.045$. Equation (36) involves four levels of ϕ_i, so that three initial levels of data are required to start off the calculation. Equation (19b) was used to locate the shock at times $xs(-\Delta t)$ and $xs(-2\Delta t)$.

The results are plotted for 49, 50, 99, and 100 iterations. Here

$$\left(\phi_x\right)_{i+1/2}^n = \left(\phi_{i+1}^n - \phi_i^n\right) / \Delta x \quad ,$$

and $\Delta x = 0.01$. The solid vertical lines show the shock position of the exact analytic answer. The results give numerical evidence that the algorithm is stable for $V_s \Delta t \leq \Delta x/2$, computes the correct shock speed and by the addition of the proper amount of artificial dissipation will produce a sharp shock profile. The ability to take a time step in which the shock moves one-half mesh spacing shows that the method allows the use of large time steps, by which we mean on the order of time steps allowed by the implicit algorithm of Ref. 6 for the low frequency, small disturbance equation. No determination of a limit on the time step size was made.

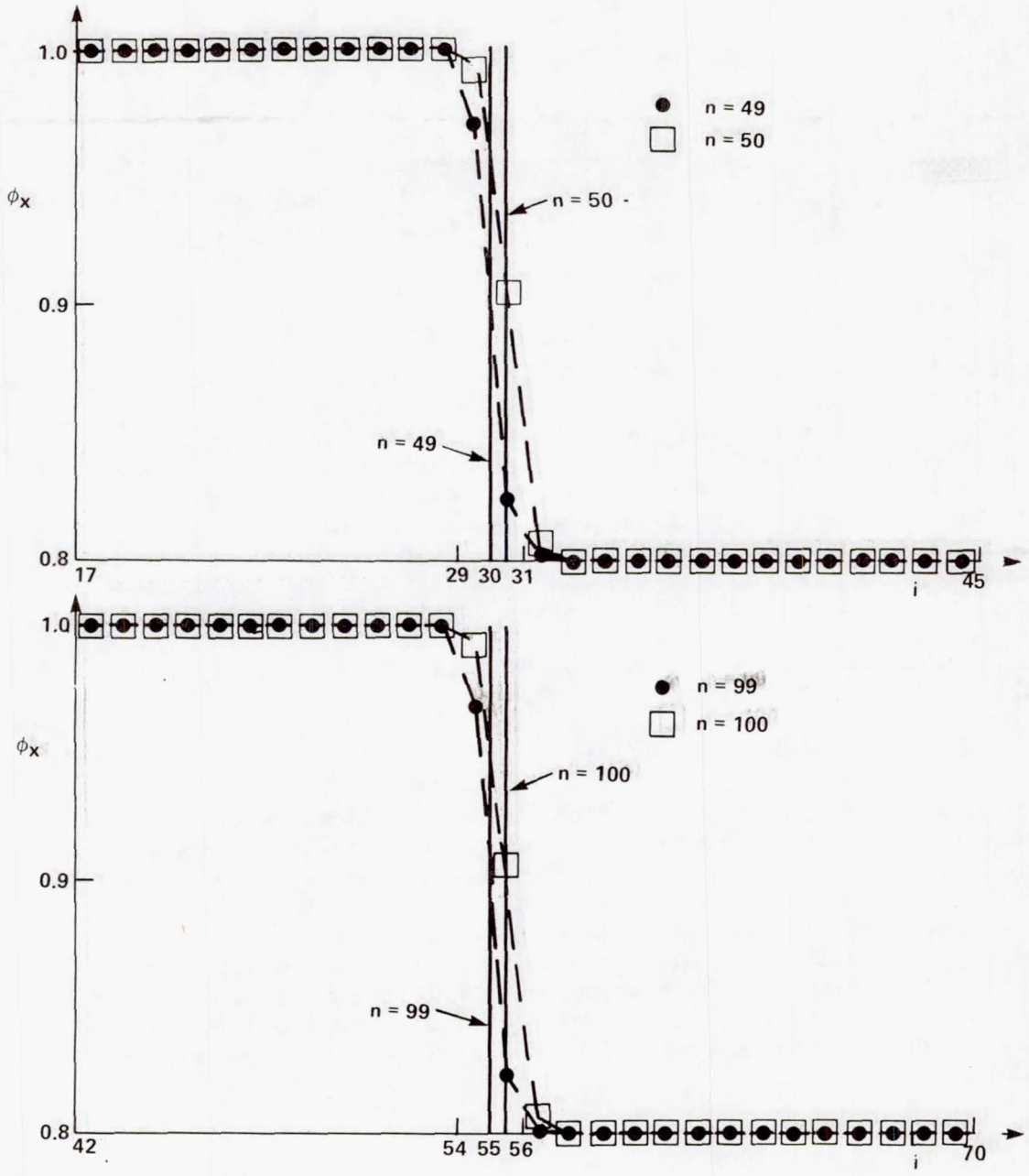

Figure 2.— Shock Profiles for One Dimensional Problem.

IV. TWO DIMENSIONAL UNSTEADY TRANSONIC FLOW

In this section we will present the results of a sample two dimensional calculation. The case presented will have no lift. However a strong shock wave will develop and subsequently travel rapidly upstream in a large excursion. Meanwhile the flow will become completely subsonic. The results will be compared with computed results from low frequency, small disturbance, transonic theory.[6]

a) Problem Formulation

We will compute the flow that results from a thickening and subsequently thinning airfoil. Here time is measured in chord lengths travelled, $k = 1$, and x and y are nondimensionalized by the chord length. A parabolic arc airfoil thickens from zero to 10 percent thick as a fluid particle travels 15 chord lengths, relative to the airfoil, at the free stream velocity q_∞. The airfoil then thins to zero thickness at 30 chord lengths of travel. Figure 3 shows the mid-chord thickness function $\delta(t)$, given by

$$\delta(t) = \begin{cases} 0.1 \left[10 - 15\left(\frac{t}{15}\right) + 6\left(\frac{t}{15}\right)^2\right]\left(\frac{t}{15}\right)^3 , & 0 \le t \le 15 , \\ 0.1 \left[10 - 15\left(\frac{30-t}{15}\right) + 6\left(\frac{30-t}{15}\right)^2\right]\left(\frac{30-t}{15}\right)^3 , & 15 \le t \le 30 , \\ 0 , & t \ge 30 . \end{cases} \tag{37}$$

For our problem we can choose a simple, sheared coordinate system (ξ, η, τ) to fit the airfoil and its motion. Equations (7) become

$$\xi = x , \qquad \eta = y - S(x,t) , \qquad \tau = t , \tag{38}$$

where

$$y = S(x,t) , \qquad 0 \le x \le 1 ,$$

is the equation of the airfoil upper surface boundary in (x, y, t) space. $S(x,t) \equiv 0$ for $x < 0$ and $x > 1$. Since the flow is symmetrical about $y = 0$, we restrict the domain of flow to $\eta \ge 0$. The governing equations simplify. $J = 1$, so the conservation of mass equation, Eq. (1), becomes

$$\frac{\partial \rho}{\partial \tau} + \frac{\partial}{\partial \xi}(\rho U) + \frac{\partial}{\partial \eta}(\rho V) = 0 , \tag{39}$$

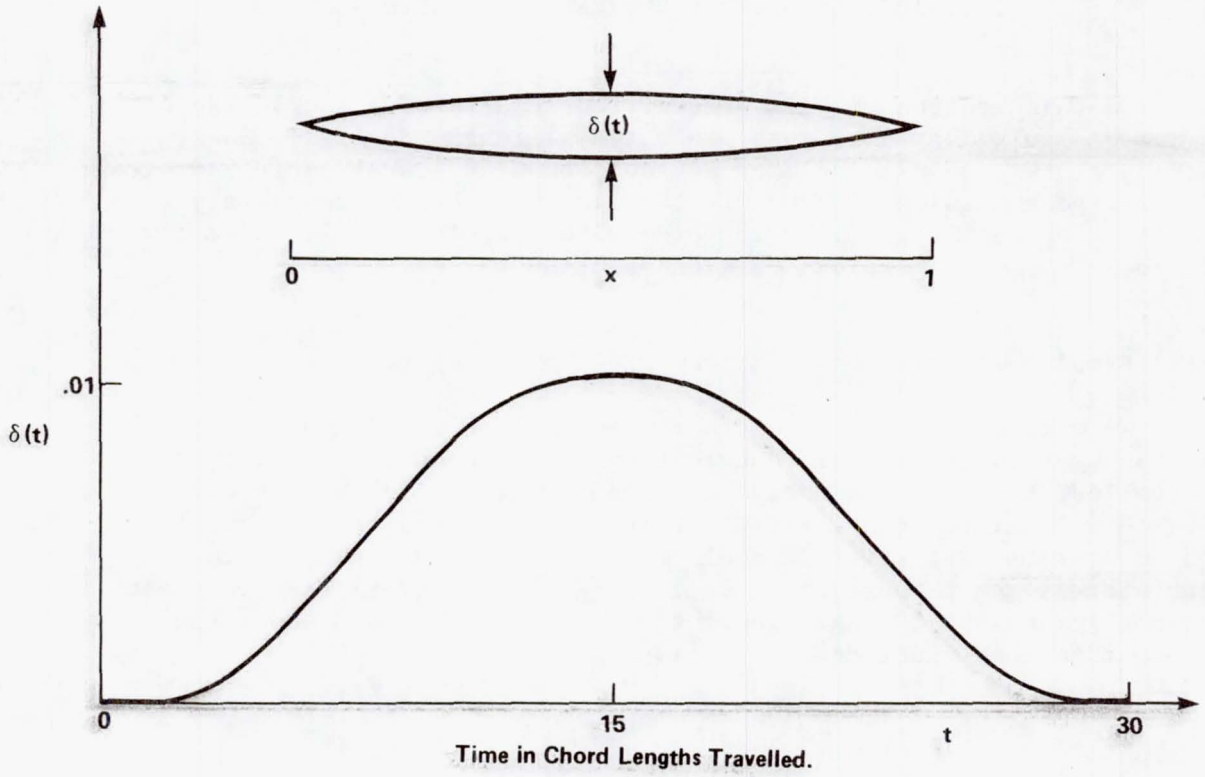

Figure 3.— Midchord Thickness Function $\delta(t)$.

where, using Eqs. (10) and (11)

$$U = u = \phi_\xi - S_x\phi_\eta = \phi_\xi - S_\xi\phi_\eta \,,$$
$$V = -S_t - S_x u + v = -S_t - S_x\phi_\xi + (1 + S_x^2)\phi_\eta = -S_\tau - S_\xi\phi_\xi + (1 + S_\xi^2)\phi_\eta \,. \tag{40}$$

The last equalities in Eqs. (40) follow from Eqs. (38); $S(x,t) = S(\xi,\tau)$, so $S_x = S_\xi$ and $S_t = S_\tau$. The unsteady Bermoulli equation, Eq. (4), becomes

$$\rho = \left[1 + M_\infty^2\left(\frac{\gamma - 1}{2}\right)\left\{1 - 2(\phi_\tau - S_\tau\phi_\eta) - \left(\phi_\xi^2 - 2S_\xi\phi_\xi\phi_\eta + (1 + S_\xi^2)\phi_\eta^2\right)\right\}\right]^{\frac{1}{\gamma - 1}} . \tag{41}$$

The initial condition is $\vec{q} = \vec{q}_\infty$ for $\tau \leq 0$. The body boundary condition, Eq. (15), becomes

$$v = S_t + S_x u \ ,$$

or

$$\phi_\eta = \frac{S_\tau + S_\xi \phi_\xi}{(1 + S_\xi^2)} \ . \tag{42}$$

Off the airfoil for $\eta = 0$, $\phi_\eta = 0$ from symmetry. In the far field $\vec{q} = \vec{q}_\infty = (u,v) = (1,0)$. From Eqs. (40)

$$u = \phi_\xi - S_x \phi_\eta = 1 \ . \tag{43}$$

From Eqs. (38), $\phi_\eta = \phi_y$, so $\phi_\eta = \phi_y = v = 0$. Substituting into Eq. (43), we have $\phi_\xi = 1$ in the far field.

For our computations, we approximate the flow on the infinite domain with the flow on a finite domain,

$$-30 \leq \xi \leq 30 \ , \qquad 0 \leq \eta \leq 50 \ . \tag{44}$$

On the far boundaries, $\eta = 50$ and $\xi = \pm 30$, we impose Dirichlet conditions, viz. ϕ is specified with the result that $\phi_\eta = 0$ on $\xi = \pm 30$ and $\phi_\xi = 1$ on $\eta = 50$. The problem formulation is now complete.

b) Implicit Factorization Algorithm

The 2-D algorithm is a generalization of the 1D differencing. Let (i,j,n) denote the indices of a mesh point located at the coordinates (ξ,η,τ) in the flow domain. Here we use a stretched computational mesh; see Fig. 4 for a sketch of the mesh. First order time accurate, implicit Euler, finite difference approximations of Eqs. (39) to (41) are

$$\overleftarrow{\delta}_\tau \rho_{i,j}^{n+1} + \overleftarrow{\delta}_\xi \left(\rho_{i+1/2,j}^{n+1} \left[\vec{\delta}_\xi \phi_{i,j}^{n+1} - S_\xi^{n+1} \ \delta_\eta \phi_{i+1/2,j}^{n+1} \right] \right)$$

$$+ \delta_\eta \left(\rho_{i,j+1/2}^{n+1} \left[\left(1 + \left(S_\xi^{n+1} \right) \delta_\eta \phi_{i,j}^{n+1} - S_\xi^{n+1} \ \delta_\xi \phi_{i,j+1/2}^{n+1} - S_\tau^{n+1} \right] \right) = 0 \ , \tag{45a}$$

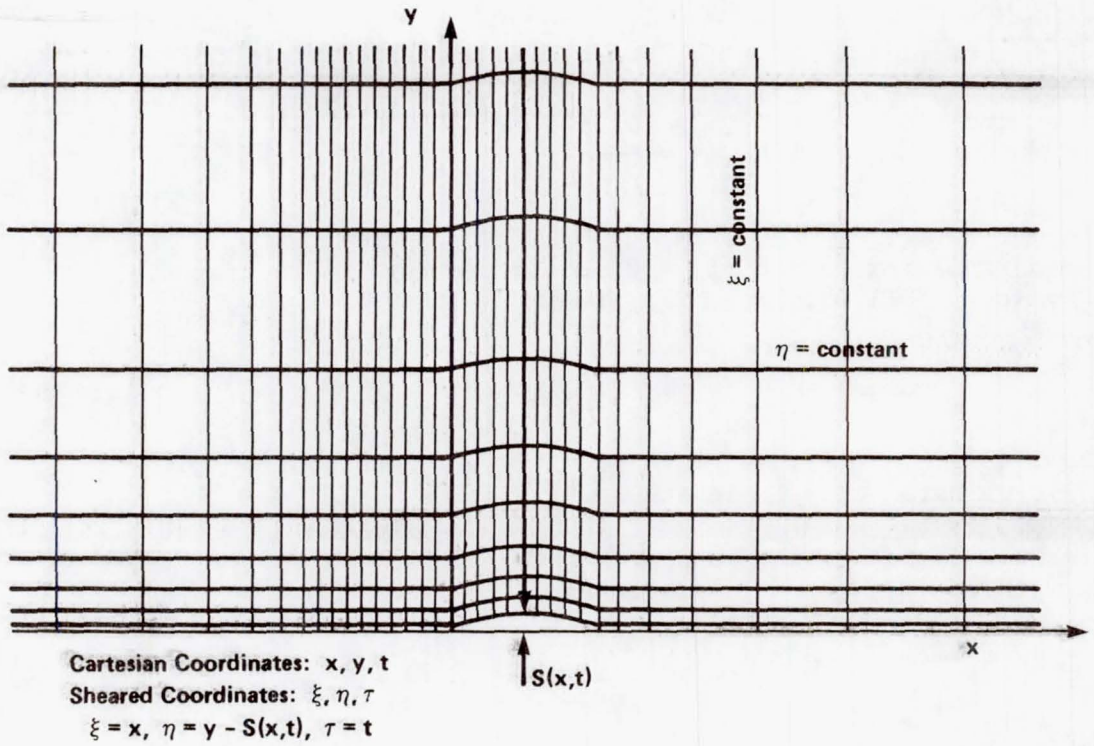

Figure 4.— Sketch of Sheared Computational Mesh.

$$\rho_{i,j}^{n+1} = \left\{1 + M_\infty^2 \left(\frac{\gamma - 1}{2}\right)\left\{1 - 2\left(\overleftarrow{\delta}_\tau \phi_{i,j}^{n+1} - S_\tau^{n+1} \delta_\eta \phi_{i,j}^{n+1}\right)\right.\right.$$

$$- \left(\left[\delta_\xi \phi_{i,j}^{n+1}\right]^2 - 2S_\xi^{n+1}\left[\delta_\xi \phi_{i,j}^{n+1}\right]\left[\delta_\eta \phi_{i,j}^{n+1}\right]\right. \tag{45b}$$

$$\left.\left. + \left[1 + \left(S_\xi^{n+1}\right)^2\right]\left[\delta_\eta \phi_{i,j}^{n+1}\right]^2\right)\right\}\Bigg]^{\frac{1}{\gamma - 1}},$$

$$\rho_{i+1/2,j}^{n+1} = \frac{1}{2}\left(\rho_{i+1,j}^{n+1} + \rho_{i,j}^{n+1}\right), \qquad \rho_{i,j+1/2}^{n+1} = \frac{1}{2}\left(\rho_{i,j+1}^{n+1} + \rho_{i,j}^{n+1}\right), \tag{45c}$$

$$\phi^{n+1}_{i+1/2,j} = \frac{1}{2}\left(\phi^{n+1}_{i,j} + \phi^{n+1}_{i+1,j}\right), \quad \phi^{n+1}_{i,j+1/2} = \frac{1}{2}\left(\phi^{n+1}_{i,j} + \phi^{n+1}_{i,j+1}\right), \tag{45d}$$

$$S^{n+1}_{\tau} = \left(S_{\tau}\right)^{n+1}_{i}, \quad S^{n+1}_{\xi} = \left(S_{\xi}\right)^{n+1}_{i}, \tag{45e}$$

where

$$\overleftarrow{\delta}_{\tau} = (\Delta\tau)^{-1}\,(1 - E_{\tau}^{-1}) \quad , \quad O(\Delta\tau)$$

$$\overleftarrow{\delta}_{\xi} = (\xi_{i} - \xi_{i-1})^{-1}\,(1 - E_{\xi}^{-1}) \quad , \quad O(\Delta\xi)$$

$$\overrightarrow{\delta}_{\xi} = (\xi_{i+1} - \xi_{i})^{-1}\,(E_{\xi}^{+1} - 1) \quad , \quad O(\Delta\xi)$$

$$\delta_{\xi} = (\xi_{i+1} - \xi_{i-1})^{-1}\,(E_{\xi}^{+1} - E_{\xi}^{-1}) \quad , \quad O(\Delta\xi^2)$$

$$\overleftarrow{\delta}_{\eta} = (\eta_{j} - \eta_{j-1})^{-1}\,(1 - E_{\eta}^{-1}) \quad , \quad O(\Delta\eta)$$

$$\overrightarrow{\delta}_{\eta} = (\eta_{j+1} - \eta_{j})^{-1}\,(E_{\eta}^{+1} - 1) \quad , \quad O(\Delta\eta)$$

$$\delta_{\eta} = (\eta_{j+1} - \eta_{j-1})^{-1}\,(E_{\eta}^{+1} - E_{\eta}^{-1}) \quad , \quad O(\Delta\eta^2)$$

The shift operators are defined by

$$E_{\tau}^{\pm 1}\,\phi^{n}_{i,j} = \phi^{n\pm 1}_{i,j} \quad ,$$

$$E_{\xi}^{\pm 1}\,\phi^{n}_{i,j} = \phi^{n}_{i\pm 1,j} \quad ,$$

$$E_{\eta}^{\pm 1}\,\phi^{n}_{i,j} = \phi^{n}_{i,j\pm 1} \quad .$$

Equations (45a) and (45b) form a system of two implicit equations at each mesh point (i,j, n+1) for the unknowns $\rho^{n+1}_{i,j}$ and $\phi^{n+1}_{i,j}$. As in the one dimensional problem we linearize backward in time the density functions in Eq. (45a), so that only the unknowns $\phi^{n+1}_{i,j}$ occur and they occur in a linear manner. Again by a Taylor series expansion we have for $\rho^{n+1}_{i,j}$ that

$$\rho^{n+1}_{i,j} = \rho^{n}_{i,j} + \left(\frac{\partial\rho}{\partial t}\right)^{n}_{i,j}\Delta t + O\left(\Delta t^2\right) .$$

Using Eq. (45b) for $\rho^n_{i,j}$, we calculate $(\partial\rho/\partial t)^n_{i,j}$ and substitute into the previous equation to obtain

$$\begin{aligned}
\rho^{n+1}_{i,j} = \rho^n_{i,j} - \Delta\tau M_\infty^2 \left(\rho^n_{i,j}\right)^{2-\gamma} \Big\{ & \overleftarrow{\delta}_\tau \left(\overleftarrow{\delta}_\tau \, \phi^{n+1}_{i,j} \right) - S^{n+1}_\tau \, \overleftarrow{\delta}_\tau \left(\delta_\eta \, \phi^{n+1}_{i,j} \right) \\
& - S^{n+1}_{\tau\tau} \, \delta_\eta \, \delta^{n+1}_{i,j} + \left(\delta_\xi \, \phi^n_{i,j} \right) \left[\overleftarrow{\delta}_\tau \left(\delta_\xi \, \phi^{n+1}_{i,j} \right) \right] \\
& - \frac{1}{2} S^{n+1}_{\xi\tau} \left[\left(\delta_\xi \, \phi^n_{i,j} \right) \left(\delta_\eta \, \phi^{n+1}_{i,j} \right) + \left(\delta_\xi \, \phi^{n+1}_{i,j} \right) \left(\delta_\eta \, \phi^n_{i,j} \right) \right] \\
& - S^{n+1}_\xi \left(\delta_\eta \, \phi^n_{i,j} \right) \left[\overleftarrow{\delta}_\tau \left(\delta_\xi \, \phi^{n+1}_{i,j} \right) \right] \\
& - S^{n+1}_\xi \left(\delta_\xi \, \phi^n_{i,j} \right) \left[\overleftarrow{\delta}_\tau \left(\delta_\eta \, \phi^{n+1}_{i,j} \right) \right] \\
& + \left(1 + \left[S^{n+1}_\xi \right]^2 \right) \left(\delta_\eta \, \phi^n_{i,j} \right) \left[\overleftarrow{\delta}_\tau \left(\delta_\eta \, \phi^{n+1}_{i,j} \right) \right] \\
& + S^{n+1}_\xi \, S^{n+1}_{\xi\tau} \left(\delta_\eta \, \phi^n_{i,j} \right) \left(\delta_\eta \, \phi^{n+1}_{i,j} \right) \Big\} + O(\Delta\tau^2) \, .
\end{aligned} \tag{46}$$

Also, in Eq. (45a) let

$$\begin{aligned}
\rho^{n+1}_{i+1/2,j} &= \rho^n_{i+1/2,j} + O(\Delta\tau) \, , \\
\rho^{n+1}_{i,j+1/2} &= \rho^n_{i,j+1/2} + O(\Delta\tau) \, .
\end{aligned} \tag{47}$$

As in the one dimensional case, the $\delta_\xi \, \phi_{i,j}$ terms in Eq. (46) are replaced by $\overleftarrow{\delta}_\xi \, \phi_{i,j}$ terms, in order to enhance the stability of the difference scheme.

The manner of adding artificial dissipation is similar to that in the one dimensional case. Again, we add an artificial dissipation term[18] by retarding upwind the density evaluation.[17,19-20] For this sample case, only densities occurring in the ξ difference term, viz, the second term in Eq. (45a), were retarded in the upwind direction. However, in general, one can retard densities upwind in both space difference terms in the manner shown in reference 19 and these achieve a rotated difference[18] scheme. Here $\rho^n_{i+1/2,j}$ is replaced by $\tilde{\rho}^n_{i+1/2,j}$, an upwinded evaluation given by

$$\tilde{\rho}^{n}_{i+1/2,j} = \left(1 - \nu^{n}_{i,j}\right) \rho^{n}_{i+1/2,j} + \nu^{n}_{i,j}\, \rho^{n}_{i-1/2,j} \,, \tag{48}$$

where

$$\nu^{n}_{i,j} = \min\left[1, \max\left\{0, \left(1 - \left[1/M^{n}_{i,j}\right]\right)c\right\}\right] \,, \tag{49}$$

where c is a positive constant, which for the computation shown was turned to 2.0 and $M^{n}_{i,j}$ is the local Mach number. Recall $M = q/a$, so

$$\left(M^{n}_{i,j}\right)^2 = \left(q^{n}_{i,j}\right)^2 / \left(a^{n}_{i,j}\right)^2 \,, \tag{50}$$

$$\left(q^{n}_{i,j}\right)^2 = \left(\delta_\xi \phi^{n}_{i,j}\right)^2 - 2\, S^{n}_{\xi} \left(\delta_\xi \phi^{n}_{i,j}\right)\left(\delta_\eta \phi^{n}_{i,j}\right) + \left(1 + (S^{n}_{\xi})^2\right)\left(\delta_\eta \phi^{n}_{i,j}\right)^2 \,, \tag{51}$$

and using Eq. 4

$$\left(a^{n}_{i,j}\right)^2 = \frac{1}{M^2_\infty} + \left(\frac{\gamma - 1}{2}\right)\left\{1 - 2\left(\overleftarrow{\delta}_\tau \phi^{n}_{i,j} - S^{n}_{\tau}\, \delta_\eta \phi^{n}_{i,j}\right) - \left(q^{n}_{i,j}\right)^2\right\} . \tag{52}$$

The (ξ, η, τ) coordinate system is sheared and therefore nonorthogonal. Hence in Eq. (39), there are two cross derivative terms, viz $-(S_\xi \phi_\eta)_\xi$ and $-(S_\xi \phi_\xi)_\eta$. In an implicit factorization algorithm, the question arises as to how to handle these terms. One would like to difference them implicitly on the assumption that such differencing would enhance the stability properties of the algorithm. However, here we will difference them explicitly. Recall that in alternating direction implicit schemes, each implicit difference equation is replaced by intermediate equations, which are typically implicit only along a single coordinate line. By differencing the cross derivative terms explicitly, the resulting intermediate equations in our algorithm will also link unknowns $\phi^{n+1}_{i,j}$ only on the same coordinate line. Hence the resulting algorithm will retain the structure of being completely vectorizable. This feature is desirable for the use of an algorithm on computers which are architecturally vector array processors. Hence in Eq. (45a) let

$$\overleftarrow{\delta}_\xi\left(\rho^{n+1}_{i+1/2,j}\left[S^{n+1}_{\xi}\, \delta_\eta \phi^{n+1}_{i+1/2,j}\right]\right) = \overleftarrow{\delta}_\xi\left(\tilde{\rho}^{n}_{i+1/2,j}\left[S^{n+1}_{\xi}\, \delta_\eta \phi^{n}_{i+1/2,j}\right]\right) + 0(\Delta\tau) \,, \tag{53}$$

$$\overleftarrow{\delta}_\eta\left(\rho^{n+1}_{i,j+1/2}\left[S^{n+1}_{\xi}\, \delta_\xi \phi^{n+1}_{i,j+1/2}\right]\right) = \overleftarrow{\delta}_\eta\left(\rho^{n}_{i,j+1/2}\left[S^{n+1}_{\xi}\, \delta_\xi \phi^{n}_{i,j+1/2}\right]\right) + 0(\Delta\tau) .$$

Substituting Eq. (46) to (48) in Eq. (45a), we have

$$\overleftarrow{\delta}_\tau \Big[\rho^n_{i,j} - \Delta\tau M_\infty^2 \left(\rho^n_{i,j}\right)^{2-\gamma} \overleftarrow{\delta}_\tau \left(\overleftarrow{\delta}_\tau \phi^{n+1}_{i,j}\right) - S^{n+1}_\tau \overleftarrow{\delta}_\tau \left(\delta_\eta \phi^{n+1}_{i,j}\right) - S^{n+1}_{\tau\tau}\, \delta_\eta \phi^{n+1}_{i,j}$$

$$+ \left(\overleftarrow{\delta}_\xi \phi^n_{i,j}\right)\left[\overleftarrow{\delta}_\tau\left(\overleftarrow{\delta}_\xi \phi^{n+1}_{i,j}\right)\right] - \frac{1}{2} S^{n+1}_{\xi\tau}\left[\left(\overleftarrow{\delta}_\xi \phi^n_{i,j}\right)\left(\delta_\eta \phi^{n+1}_{i,j}\right) + \left(\overleftarrow{\delta}_\xi \phi^{n+1}_{i,j}\right)\left(\delta_\eta \phi^n_{i,j}\right)\right]$$

$$- S^{n+1}_\xi \left(\delta_\eta \phi^n_{i,j}\right)\left[\overleftarrow{\delta}_\tau\left(\overleftarrow{\delta}_\xi \phi^{n+1}_{i,j}\right)\right] - S^{n+1}_\xi \left(\overleftarrow{\delta}_\xi \phi^n_{i,j}\right)\left[\overleftarrow{\delta}_\tau\left(\delta_\eta \phi^{n+1}_{i,j}\right)\right] \tag{54}$$

$$+ \left(1 + (S^{n+1}_\xi)^2\right)\left(\delta_\eta \phi^n_{i,j}\right)\left[\overleftarrow{\delta}_\tau\left(\delta_\eta \phi^{n+1}_{i,j}\right)\right] + S^{n+1}_\xi S^{n+1}_{\xi\tau}\left(\delta_\eta \phi^n_{i,j}\right)\left(\delta_\eta \phi^{n+1}_{i,j}\right)\Big\}\Big]$$

$$+ \overleftarrow{\delta}_\xi\left(\widetilde{\rho}^n_{i+1/2,j}\left[\overrightarrow{\delta}_\xi \phi^{n+1}_{i,j} - S^{n+1}_\xi\, \delta_\eta \phi^n_{i+1/2,j}\right]\right)$$

$$+ \overleftarrow{\delta}_\eta\left(\rho^n_{i,j+1/2}\left[\left(1 + (S^{n+1}_\xi)^2\right)\overrightarrow{\delta}_\eta \phi^{n+1}_{i,j} - S^{n+1}_\xi\, \delta_\xi \phi^n_{i,j+1/2} - S^{n+1}_\tau\right]\right) = 0 \ .$$

Note Eq. (54) is in conservation form and $\phi^{n+1}_{i,j}$ occurs in a linear manner. We now shall factor Eq. (54). Note Eq. (45b) is used to evaluate the density at the previous time levels.

By algebraic operations, Eq. (54) is transformed into the form:

$$L^n_{i,j}\, \phi^{n+1}_{i,j} = \phi^{n+1}_{i,j} + A\overleftarrow{\delta}_\xi \phi^{n+1}_{i,j} + B\,\delta_\eta \phi^{n+1}_{i,j} + C\overleftarrow{\delta}_\xi\left(\widetilde{\rho}^n_{i+1/2,j}\, \overrightarrow{\delta}_\xi \phi^{n+1}_{i,j}\right)$$

$$+ C\overleftarrow{\delta}_\eta\left(\rho^n_{i,j+1/2}\left(1 + \left(S^{n+1}_\xi\right)^2\right)\overrightarrow{\delta}_\eta \phi^{n+1}_{i,j}\right) = R \ , \tag{55}$$

where

$$A = A1 + A2 \ ,$$

$$A1 = \Delta\tau\left(\overleftarrow{\delta}_\xi \phi^n_{i,j} - S^{n+1}_\xi\, \delta_\eta \phi^n_{i,j}\right) \ ,$$

$$A2 = -\Delta\tau^2 \frac{1}{2} S^{n+1}_{\xi\tau}\, \delta_\eta \phi^n_{i,j} \ ,$$

$$B = B1 + B2 \ ,$$

$$B1 = \Delta\tau\left[1 + \left(S^{n+1}_\xi\right)^2\right]\delta_\eta \phi^n_{i,j} - S^{n+1}_\xi \overleftarrow{\delta}_\xi \phi^n_{i,j} - S^{n+1}_\tau \ ,$$

$$B2 = \Delta\tau^2\left(S_{\xi\tau}^{n+1}\left(S_{\xi}^{n+1}\,\delta_\eta\,\phi_{i,j}^{n}\right) - \frac{1}{2}\,\overleftarrow{\delta}_\xi\,\phi_{i,j}^{n}\right) - S_{\tau\tau}^{n+1}\ ,$$

$$C = -\Delta\tau^2/M_\infty^2\left(\rho_{i,j}^{n}\right)^{2-\gamma}$$

$$\overline{A} = \overline{A1} + \overline{A2}$$

$$\overline{A1} = E_\tau^{-1}(A1),\ \overline{A2} = E_\tau^{-1}(A2),\ \overline{B1} = E_\tau^{-1}(B1)\ ,$$

$$\overline{B2} = E_\tau^{-1}(B2),\ \overline{C} = E_\tau^{-1}(C)\ ,$$

$$R = 2\,\phi_{i,j}^{n} - \phi_{i,j}^{n-1} + (A1)\,\overleftarrow{\delta}_\xi\,\phi_{i,j}^{n} + (B1)\,\delta_\eta\,\phi_{i,j}^{n}$$

$$+ \frac{1}{\left(\rho_{i,j}^{n}\right)^{2-\gamma}}\left\{\frac{\Delta\tau}{M_\infty^2}\left(\rho_{i,j}^{n} - \rho_{i,j}^{n-1}\right) + \left(\rho_{i,j}^{n-1}\right)^{2-\gamma}\left[\phi_{i,j}^{n} - 2\phi_{i,j}^{n-1}\right.\right.$$

$$+ \phi_{i,j}^{n-1} + \overline{A1}\,(\Delta\tau)\,\overleftarrow{\delta}_\tau\left(\overleftarrow{\delta}_\xi\,\phi_{i,j}^{n}\right) + \overline{B1}(\Delta\tau)\,\overleftarrow{\delta}_\tau\left(\delta_\eta\,\phi_{i,j}^{n}\right)$$

$$\left.\left. + \overline{A2}\,\overleftarrow{\delta}_\xi\,\phi_{i,j}^{n} + \overline{B2}\,\delta_\eta\,\phi_{i,j}^{n}\right]\right\} + C\,\overleftarrow{\delta}_\xi\left(\tilde{\rho}_{i+1/2,j}^{n+1}\,S_{\xi}^{n+1}\,\delta_\eta\,\phi_{i+1/2,j}^{n}\right)$$

$$+ C\,\overleftarrow{\delta}_\eta\left(\rho_{i,j+1/2}^{n+1/2}\left[S_{\xi}^{n+1}\,\delta_\xi\,\phi_{i,j+1/2}^{n} + S_{\tau}^{n+1}\right]\right).$$

Equation (55) is an implicit equation that determines $\phi_{i,j}^{n+1}$. We wish to factor the operator $L_{i,j}^{n}$ to obtain two intermediate equations at each mesh point. Each intermediate set of equations will be implicit in only one coordinate direction. The resulting matrix equations will be tridiagonal and can be easily inverted by use of the Thomas algorithm.[21] The factorization of the operators $L_{i,j}^{n}$ will be approximate; however, the resulting additional terms will only be error terms that are of higher order error in time than the discretization errors already made. Also, some of the error terms will not be in conservation form. Therefore additional terms will be added at the nth time level to recover the conservation form for the factored equation.

The factorization of Eq. (55) is

ξ implicit sweep

$$\phi^*_{i,j} + A\overleftarrow{\delta}_\xi \phi^*_{i,j} + C\overleftarrow{\delta}_\xi\left(\tilde{\rho}^n_{i+1/2,j}\overrightarrow{\delta}_\xi \phi^*_{i,j}\right)$$

$$= R - B\delta_\eta \phi^n_{i,j} - C\overleftarrow{\delta}_\eta\left(\rho^n_{i,j+1/2}\left(1 + \left(S^{n+1}_\xi\right)^2\right)\overrightarrow{\delta}_\eta \phi^n_{i,j}\right) + CD \ , \tag{56a}$$

η implicit sweep

$$\phi^{n+1}_{i,j} + B\delta_\eta \phi^{n+1}_{i,j} + C\overleftarrow{\delta}_\eta\left(\rho^n_{i,j+1/2}\left(1 + \left(S^{n+1}_\xi\right)^2\right)\overrightarrow{\delta}_\eta \phi^{n+1}_{i,j}\right)$$

$$= \phi^*_{i,j} + B\delta_\eta \phi^n_{i,j} + C\overleftarrow{\delta}_\eta\left(\rho^n_{i,j+1/2}\left(1 + \left(S^{n+1}_\xi\right)^2\right)\overrightarrow{\delta}_\eta \phi^n_{i,j}\right) \ , \tag{56b}$$

where the term CD is added to the right side in the ξ sweep in order to maintain conservation form and

$$D = \frac{\Delta\tau\overline{A}}{\overline{C}}\overleftarrow{\delta}_\xi\left[\overline{B}\delta_\eta\overleftarrow{\delta}_\tau \phi^n_{i,j} + \overline{C}\overleftarrow{\delta}_\eta\left(\rho^{n-1}_{i,j+1/2}\left(1 + (S^n_\xi)^2\right)\overrightarrow{\delta}_\eta\overleftarrow{\delta}_\tau \phi^n_{i,j}\right)\right] \ . \tag{56c}$$

Note that the ξ implicit sweep is not a consistent approximation to Eq. (39) because of the replacement of the term $B\delta_\eta \phi^{n+1}_{i,j}$ in Eq. (55) by the term $B\delta_\eta \phi^n_{i,j}$ in Eq. (56a). Equations (56) are a generalization of the alternating direction implicit (ADI) algorithm of Lees.[21] Equation (56b) can be solved for $\phi^*_{i,j}$. The resulting expression can be substituted into Eq. (56a) to yield

$$\phi^{n+1}_{i,j} + A\overleftarrow{\delta}_\xi \phi^{n+1}_{i,j} + B\delta_\eta \phi^{n+1}_{i,j} + C\overleftarrow{\delta}_\xi\left(\tilde{\rho}^n_{i+1/2,j}\overrightarrow{\delta}_\xi \phi^{n+1}_{i,j}\right)$$

$$+ C\overleftarrow{\delta}_\eta\left(\rho^n_{i,j+1/2}\left(1 + (S^{n+1}_\xi)^2\right)\overrightarrow{\delta}_\eta \phi^{n+1}_{i,j}\right)$$

$$+ \Delta\tau C\overleftarrow{\delta}_\xi\left(\tilde{\rho}^n_{i+1/2,j}\overrightarrow{\delta}_\xi\left[B\delta_\eta\overleftarrow{\delta}_\tau \phi^{n+1}_{i,j} + C\overleftarrow{\delta}_\eta\left(\rho^n_{i,j+1/2}\left(1 + (S^{n+1}_\xi)^2\right)\overrightarrow{\delta}_\eta\overleftarrow{\delta}_\tau \phi^{n+1}_{i,j}\right)\right]\right) \tag{57}$$

$$+ \Delta\tau A\overleftarrow{\delta}_\xi\left[B\delta_\eta\overleftarrow{\delta}_\tau \phi^{n+1}_{i,j} + C\overleftarrow{\delta}_\eta\left(\rho^n_{i,j+1/2}\left(1 + (S^{n+1}_\xi)^2\right)\overrightarrow{\delta}_\eta\overleftarrow{\delta}_\tau \phi^{n+1}_{i,j}\right)\right]$$

$$= R + CD \ .$$

Equation (57) is an approximation to Eq. (55); there are two additional terms on the left side, which resulted from the splitting and there is the additional term CD on the right side. Division Eq. (57) by the factor C and rearrangement of the terms results in the equation:

$$T1 + T2 + T3 = 0 \ , \tag{58}$$

where T1 is all the terms on the left side of Eq. (54),

$$T2 = \Delta\tau \overleftarrow{\delta}_\xi \left(\tilde{\rho}^{\,n}_{i+1/2,j} \overrightarrow{\delta}_\xi \left[B\, \delta_\eta \overleftarrow{\delta}_\tau \phi^{n+1}_{i,j} + C \overleftarrow{\delta}_\eta \left(\rho^{n}_{i,j+1/2} \left(1 + \left(S^{n+1}_{\xi} \right)^2 \right) \overrightarrow{\delta}_\eta \overleftarrow{\delta}_\tau \phi^{n+1}_{i,j} \right) \right] \right) \ , \tag{59}$$

and

$$T3 = \Delta\tau \frac{A}{C} \overleftarrow{\delta}_\xi \left[B\, \delta_\eta \overleftarrow{\delta}_\tau \phi^{n+1}_{i,j} + C \overleftarrow{\delta}_\eta \left(\rho^{n}_{i,j+1/2} \left(1 + \left(S^{n+1}_{\xi} \right)^2 \right) \overrightarrow{\delta}_\eta \overleftarrow{\delta}_\tau \phi^{n+1}_{i,j} \right) \right] - D. \tag{60}$$

Using Eq. (56c)

$$T3 = (\Delta\tau)^2 \overleftarrow{\delta}_\tau \left\{ \frac{A}{C} \overleftarrow{\delta}_\xi \left[B\, \delta_\eta \overleftarrow{\delta}_\tau \phi^{n+1}_{i,j} + C \overleftarrow{\delta}_\eta \left(\rho^{n}_{i,j+1/2} \left(1 + \left(S^{n+1}_{\xi} \right)^2 \right) \overrightarrow{\delta}_\eta \overleftarrow{\delta}_\tau \phi^{n+1}_{i,j} \right) \right] \right\} . \tag{61}$$

From the difference form of the terms T1, T2, T3, given in Eqs. (54), (59) and (61), we see that Eq. (58) is in conservation form, including the error terms, T2 and T3. Solutions of Eq. (57) are identical to solutions of Eq. (58), since only arithmetic operations are required to go from one equation to the other. Hence solutions of Eq. (57) will satisfy the conservative form, finite difference approximation, Eq. (58), to the conservation of mass differential equation.

Since $A = 0(\Delta\tau)$, $B = 0(\Delta\tau)$ and $C = 0(\Delta\tau^2)$, it follows from Eqs. (59) and (61) that $T2 = 0(\Delta\tau^2)$ and $T3 = 0(\Delta\tau^2)$. So the additional error terms in Eq. (58) do not affect the first order accuracy in time of the finite difference approximation.

The addition of the term CD in Eq. (56a) is required because the term $\Delta\tau A \overleftarrow{\delta}_\xi \phi^{*}_{i,j}$ in that equation produces error terms which are in nonconservative form. One alternative, which would eliminate that term from Eq. (56a), is to replace the term $\delta_\xi \phi^{n+1}_{i,j}$ in Eq. (46) by $\delta_\xi \phi^{n}_{i,j}$. However in the problem under consideration, that replacement resulted in an unstable algorithm. Another alternative is to interchange the order of the sweep directions in Eqs. (56) and also to replace $\delta_\eta \phi^{n+1}_{i,j}$ by $\delta_\eta \phi^{n}_{i,j}$ in Eq. (46). The rationale is that the ξ coordinate direction is approximately the flow direction in the supersonic region about an airfoil. For stability, in such regions, the $\delta_\xi \phi_{i,j}$ term must be differenced

implicitly. However the $\delta_\eta \phi_{i,j}$ term might be differenced explicitly and yet the algorithm would remain stable. The change in order of the ξ and η sweeps results in $\tilde{\rho}^n_{i+1/2,j}$ appearing in both sweeps. Hence the test for supersonic flow, Eq. (49), must be applied in both sweeps with resulting additional computations. However, in a rotated difference scheme,[18] the density $\rho^n_{i,j+1/2}$ appearing in the δ_η difference term would also be upwind biased, so that interchanging the order of the sweeps would not introduce any additional testing. This second alternative has not yet been tested.

c) Calculated Results

The calculations were performed by solving Eqs. (45b) and (56) on the computational mesh. For the case shown, the mesh had 151 points in the ξ direction and 41 points in the η direction. There were 101 mesh points in the ξ direction between $\xi = -1$ and $\xi = +1$ at a uniform spacing of $\Delta\xi = 0.02$. The remainder of the ξ mesh on either end was smoothly exponentially stretched to the boundaries at $\xi = \pm 30$ chord lengths. The mesh in the η direction was smoothly, exponentially stretched to the far field boundary at $\eta = 50$ chord lengths. At $j = 7$, $\eta_j = 0.18$ and $\Delta\eta_j = (\eta_{j+1} - \eta_{j-1})/2 \cong 0.05$. So this mesh is very similar to the mesh used in Ref. 6 for the low frequency, small disturbance, transonic equation calculations. See Appendix B for a list of the computational mesh.

As in the one dimensional case, three levels of initial data are required to advance the potential in time. The initial values $\phi^n_{i,j}$ were determined by setting $\phi^n_{1,j} = 0$ and requiring $\delta_\xi \phi^n_{i,j} = 1$. Then we set $\phi^n_{i,j} = \phi^{n-1}_{i,j} = \phi^{n-2}_{i,j}$. The boundary condition on the airfoil, Eq. (42) was imposed by the first order accurate approximation.

$$(\phi_\eta)^{n+1}_{i,1} = \frac{S_\tau^{n+1} + S_\xi^{n+1}\, \delta_\xi \phi^n_{i,1}}{1 + (S_\xi^{n+1})^2} , \tag{62}$$

where $j = 1$ mesh points lie on the coordinate line on the airfoil. Note that Eq. (62) is explicit in $\phi_{i,1}$. Off the airfoil, $(\phi_\eta)^{n+1}_{i,1} = 0$ was applied. At the far field boundaries, $i = 1$, $i = 151$ or $j = 41$, $\phi_{i,j}$ was not changed from the initial values, with the result that $\delta_\eta \phi^n_{i,j} = 0$ on $i = 1$ and $i = 151$ and $\delta_\xi \phi^n_{i,j} = 1$ on $j = 41$ for all values of n. In our calculations $M_\infty = 0.85$ and $\Delta_\tau = 0.0625$.

The pressure coefficients resulting from the calculation are plotted in Figs. 5 and 6. The airfoil is thickening for $\tau \leq 15$, as shown in Fig. 3, and in Fig. 5 we see that the effect of that thickening is the initial formation and downstream propagation of the shock wave. By $\tau = 8.5$, the flow has a small region of supersonic flow but there is no shock wave yet. By $\tau = 11.5$ a shock wave has formed; it is growing stronger and is moving downstream as the airfoil continues to thicken. At $\tau = 18.25$ the shock has slowed down and is nearly stationary. The local Mach number upstream

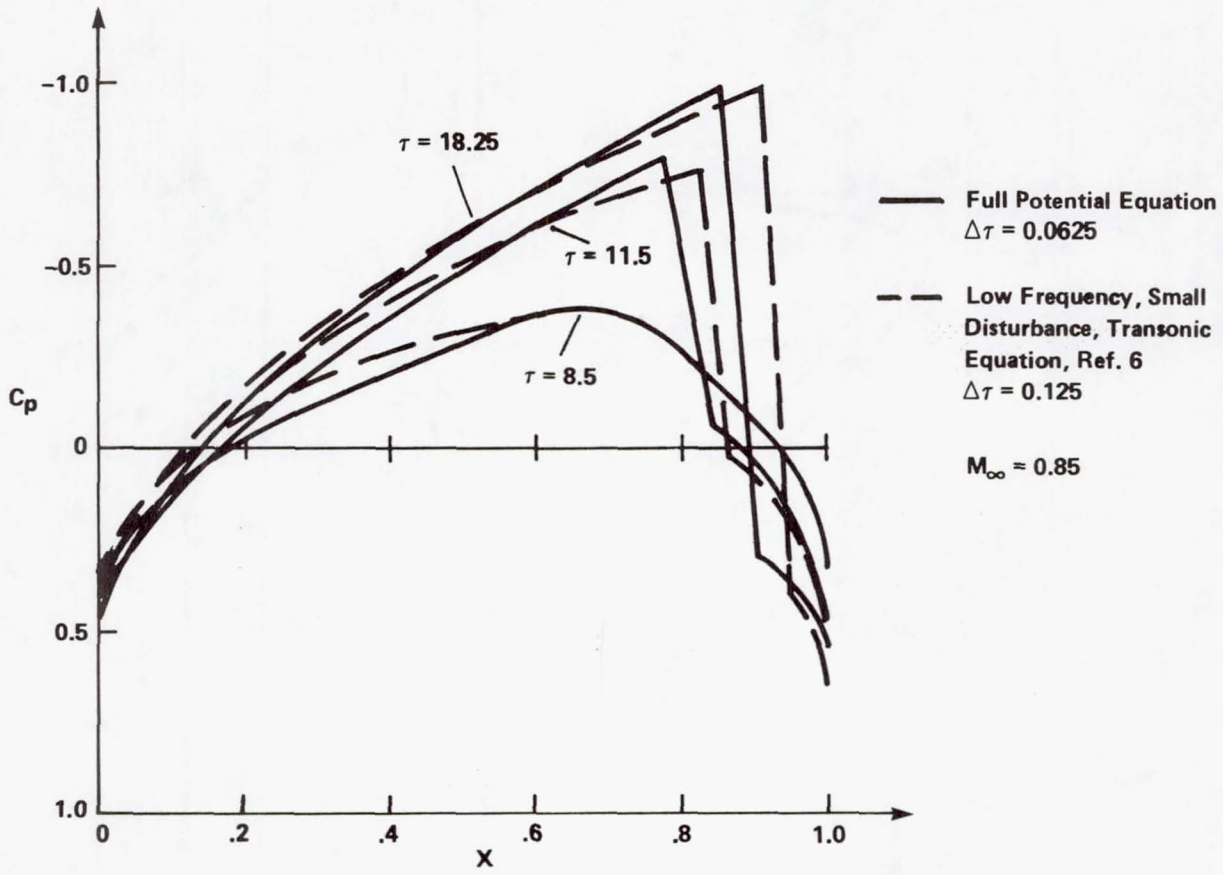

Figure 5.— Plot of Pressure Coefficients for Formulation and Downstream Propagation of the Shock Wave.

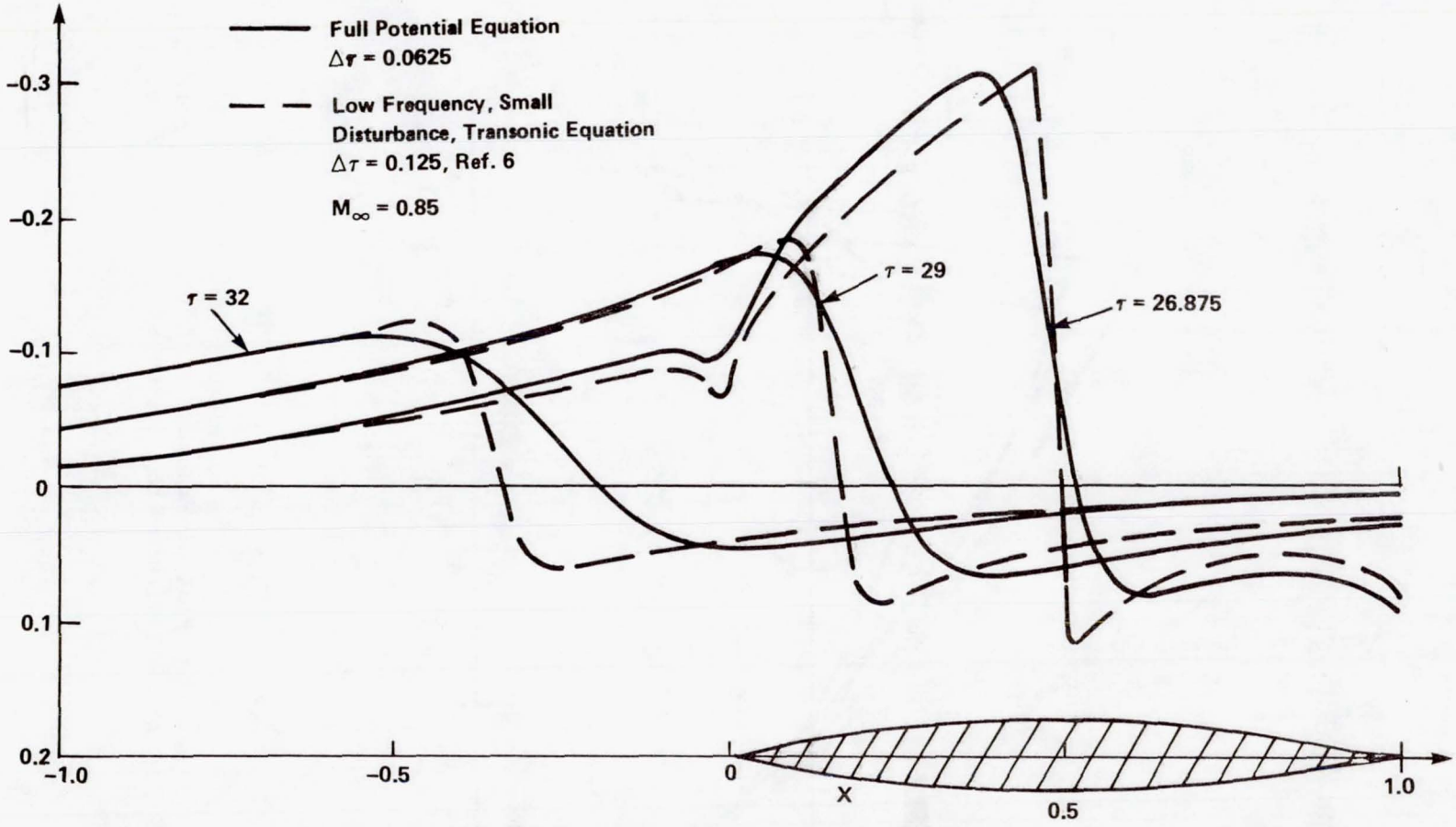

Figure 6.— Plot of Pressure Coefficients for Upstream Propagation of the Shock Wave.

of the shock, measured relative to the airfoil frame of reference, is approximately 1.38. Notice that the shock profiles are captured sharply by the algorithm. There was a time lag of about $\Delta\tau = 3.25$ between the time of the maximum thickness of the airfoil at $\tau = 15$ and the time of the shock strength reaching its maximum.

The subsequent upstream movement of the shock wave is shown in Fig. 6. At $\tau = 26.875$ the flow has just become completely subsonic and the shock is now traveling rapidly upstream. The rapid excursion is shown by the plots at $\tau = 29$ and $\tau = 32$. In Fig. 6, the shock wave is from subsonic to subsonic flow and its strength is very weak compared to the shocks in Fig. 5. Since the computation of the density is no longer upwind biased during this later completely subsonic flow, the result is that the algorithm increasingly smears the shock profile. A calculation with a time step reduced to $\Delta\tau = 0.03125$ sharpened these weak shock profiles at $\tau = 29$ and 32. They appeared similar in shape to the low frequency, small disturbance profiles plotted in Fig. 6 but they were positioned near the centers of the full potential shock profiles. At $\tau = 11.5$ and 18.25, the smaller time step calculation showed minor changes in the C_p profiles from the larger time step full potential calculation. The shock positions were moved slightly rearward and the shock strengths were slightly increased for the smaller time step case.

Another view of the solution is given in Fig. 7, which is a plot of the midchord pressure coefficient as a function of time. There is a lag of about $\Delta\tau = 2.75$ between the maximum airfoil thickness and the maximum flow expansion time. The sharp drop in the curve occurs as the shock wave propagates upstream past the midchord point at about $\tau = 26.6$.

There are no published results on unsteady, conservative, full potential, transonic calculations with which we can compare. Therefore we have compared our results with low frequency, small disturbance, transonic theory.[6] The purpose of the comparison is twofold. First, for this problem, the two theories should be in close agreement. By comparison in Figs. 5, 6 and 7, we conclude that they are in close agreement and therefore that there are no gross errors in the full potential calculations.

The second purpose of the comparison is to see how the results of the two theories differ. Notice that at times $\tau = 11.5$ and $\tau = 18.25$, the low frequency, small disturbance, transonic shocks are rearward of the full potential shocks, whereas at $\tau = 26.875$ they are in close agreement. Solutions in small disturbance, transonic theory can be adjusted in various ways, such as by Krupp, Von Karman-Spreiter, or C_p^* scaling.[7,22-24] In our comparisons, C_p^* scaling was used in the small disturbance calculations. In that scaling, the small disturbance critical pressure coefficient, C_p^*, is equal to the steady full potential critical pressure coefficient. The result is that for steady flows that are barely supercritical, the resulting shock strengths and positions should be in close agreement. In Ref. 25, a plot shows a comparison of shock positions versus airfoil thickness for steady flows at a fixed Mach number between full potential theory and small disturbance theory. There C_p^* scaling

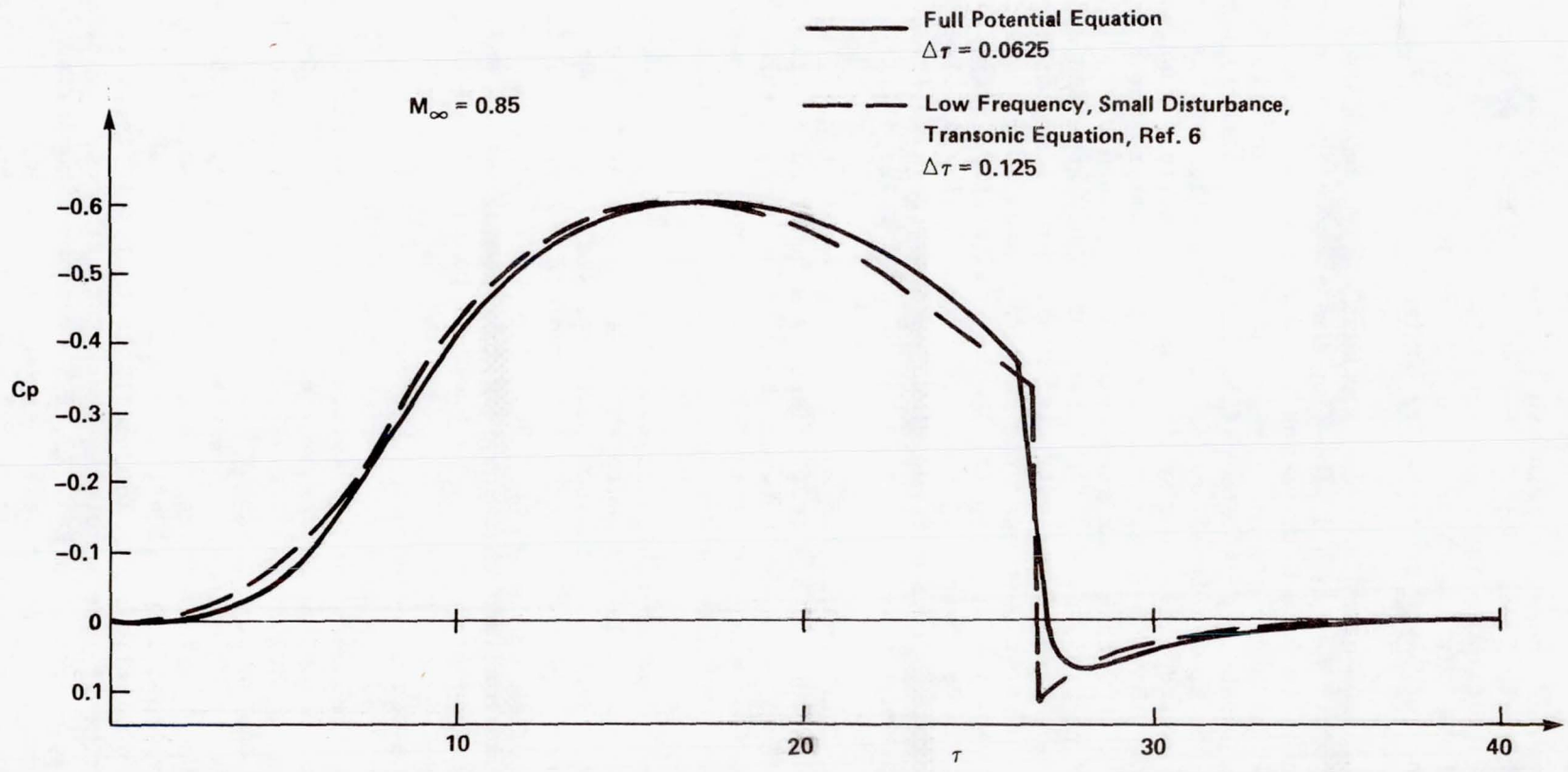

Figure 7.— Plot of Midchord Pressure Coefficient Versus Time.

was also used. That plot shows that the small disturbance shock position is rearward of the full potential shock position and that the separation increases as the thickness increases. Our comparison at $\tau = 11.5$ and 18.25 shows the same relative position of the shocks. Also there is an increase in the separation of the two shocks at the later time, which can be attributed to a greater thickness effect if one allows for the time lag between the motion of the airfoil and the reaction of the fluid. At $\tau = 26.875$, the small disturbance flow is barely supercritical and the shocks have essentially the same strength and position, which is what would be expected from using C_p^* scaling in a steady flow.

A more detailed comparison of the two theories is made in Appendix C. There the effects on the pressure coefficient plots are shown for various approximations made to full potential theory in going to small disturbance theory. The approximations studied are modelling the airfoil as a slit, linearizing the boundary condition and linearizing the formula for C_p.

V. CONCLUDING REMARKS

An algorithm has been developed which solves the two dimensional, conservative, full potential equation for unsteady, transonic flow by a finite-difference, alternating-direction implicit method. This development was motivated by the desire to remove three limitations of low-frequency, small-disturbance, transonic theory while retaining the computational efficiency and shock-capturing features of algorithms developed for that equation. This removal is necessary for an accurate treatment of thick, blunt nosed supercritical airfoils. A noteworthy new feature of the algorithm is the reduction of the system of two equations to be solved at each mesh point for the velocity potential and density functions to one equation involving only the unknown velocity potential.

By first testing the algorithm on a one-dimensional traveling shock wave, we found, as shown in Figure 2, that the algorithm is stable, captures the weak solution shock motion correctly and allows relatively large time steps, similar in size to those permitted by the small-disturbance algorithm. Next we calculated a two-dimensional flow that was produced by a thickening and thinning airfoil. That test case, as shown in Figures 5-7, also is stable, allows large time steps, and is in close agreement with low-frequency, small-disturbance transonic equation calculations as required for this test case.

Further work is underway. (1) A pilot code for use in the aerodynamic community, is being prepared which treats arbitrarily shaped airfoils using an efficient body fitted mesh[17] and which allows for pitching and plunging airfoil motions. This code will be capable of providing the unsteady loads for flutter and other aeroelastic calculations on both conventional and supercritical airfoils. (2) The algorithm is being extended to three space dimensions. (3) A modification to the algorithm is being investigated which would make the body boundary condition computation implicit. This modification could permit the use of even larger time steps.

ACKNOWLEDGEMENT

I wish to thank W. F. Ballhaus, NASA—Ames Research Center for suggesting to me the idea of time linearizing the density function in the time difference. Also I wish to thank him and T. L. Holst, NASA—Ames Research Center, for many helpful discussions throughout the development of this algorithm.

APPENDIX A

DERIVATION OF THE GOVERNING EQUATION IN A GENERAL CURVILINEAR COORDINATE SYSTEM

The conservation of mass equation, Eq. (1) is written in cartesian coordinates (t,x,y) as:

$$\frac{\partial(k\rho)}{\partial t} + \frac{\partial(\rho u)}{\partial x} + \frac{\partial(\rho v)}{\partial y} = 0 \ , \tag{A1}$$

where $\vec{q} = (u,v)$ is the velocity vector in (x,y) space. We shall use tensor analysis[26-28] to write this equation in a general coordinate system. In Euclidean space time, the line element ds^2 in the Euclidean coordinates (t,x,y) is

$$ds^2 = dt^2 + dx^2 + dy^2 \ . \tag{A2}$$

To simplify the expressions that follow, we introduce tensor notation, for use in this appendix only. The coordinates of a point in space time will be denoted x^μ, where the superscript μ takes values 1, 2 or 3. Hence $(t,x,y) = (x^1,x^2,x^3)$. In tensor notation the line element ds^2 has the form

$$ds^2 = g_{\alpha\beta}\, dx^\alpha dx^\beta \ , \tag{A3}$$

where $g_{\alpha\beta} = \delta_{\alpha\beta}$; here $\delta_{\alpha\beta}$ is the Kronecker delta function, and $\delta_{\alpha\beta} = 1$ if $\alpha = \beta$ and $\delta_{\alpha\beta} = 0$ if $\alpha \neq \beta$. In Eq. (A3) we have used the Einstein summation convention, which assumes summation on "an index which appears twice in the general term."[28] Hence in Eq. (A3) we sum on both α and β through the values 1 to 3. $g_{\alpha\beta}$ are the components of the metric tensor.

Now consider the general transformation of coordinates

$$\tau = \tau(t,x,y), \quad \xi = \xi(t,x,y), \quad \eta = \eta(t,x,y) \ . \tag{A4}$$

Let $\bar{x}^\mu$ denote the coordinates of a point in this coordinate system, so $(\bar{x}^1,\bar{x}^2,\bar{x}^3) = (\tau,\xi,\eta)$ and Eq. (A4) simplifies to $\bar{x}^\mu = \bar{x}^\mu(x^\nu)$. Then the line element ds^2 in the $\bar{x}^\mu$ coordinate system is

$$ds^2 = \bar{g}_{\mu\nu}\, d\bar{x}^\mu\, d\bar{x}^\nu \ . \tag{A5}$$

Eq. (A5) follows from the use of the inverse transformation $x^\mu = x^\mu(\bar{x}^\nu)$ so that

$$dx^\alpha = \frac{\partial x^\alpha}{\partial \bar{x}^\mu}\, d\bar{x}^\mu \ . \tag{A6}$$

Using Eq. (A6) in Eq. (A3) gives Eq. (A5) with

$$\bar{g}_{\mu\nu} = g_{\alpha\beta} \frac{\partial x^{\alpha}}{\partial \bar{x}^{\mu}} \frac{\partial x^{\beta}}{\partial \bar{x}^{\nu}} = \sum_{\alpha=1}^{3} \frac{\partial x^{\alpha}}{\partial \bar{x}^{\mu}} \frac{\partial x^{\alpha}}{\partial \bar{x}^{\nu}} \ . \tag{A7}$$

Now we shall write the conservation of mass equation in a general coordinate system. Using the velocity vector $\vec{q} = (u,v)$ we form the contravarient components V^{μ} of the velocity vector in space time in Euclidean coordinates (t,x,y).

$$V^{\mu} = (k,u,v) \ . \tag{A8}$$

Also the gradient operator in (t,x,y) space time is defined by

$$\partial_{\mu} = (\partial_t, \partial_x, \partial_y) \ . \tag{A9}$$

So in tensor notation, Eq. (A1) becomes

$$\partial_{\mu} (\rho V^{\mu}) = 0 \ . \tag{A10}$$

Under the general transformation $\bar{x}^{\mu} = \bar{x}^{\mu}(x^{\nu})$, Eq. (A10) takes the covarient form

$$\bar{\partial}_{\mu} \left(\frac{\rho \bar{V}^{\mu}}{|J|} \right) = 0 \ , \tag{A11}$$

where $|J|$ is the absolute value of the Jacobian of the transformation.

$$J = \det \left(\frac{\partial \bar{x}^{\mu}}{\partial x^{\nu}} \right) . \tag{A12}$$

$\partial \bar{x}^{\mu} / \partial x^{\nu}$ is the transformation matrix. V^{μ} are the contravarient components of the space time velocity vector in the $\bar{x}^{\mu}$ coordinate system,

$$\bar{V}^{\mu} = \frac{\partial \bar{x}^{\mu}}{\partial x^{\nu}} V^{\nu} \ . \tag{A13}$$

Note that Eq. (A11) is in conservation form. This form follows from an application of the fundamental Ricci theorem[28] to the equation that results when the transformation of coordinates, Eq. (A4), is applied to Eq. (A10). The Ricci theorem states that the covarient derivative of the metric tensor is identically zero.

If $\tau(t,x,y) = t$, then the following simplifications result.

$$J = \xi_x \eta_y - \xi_y \eta_x \quad , \tag{A14}$$

$$\bar{V}^1 = k \quad ,$$

$$U \equiv \bar{V}^2 = \xi_t + \xi_x u + \xi_y v \ ,$$

$$V \equiv \bar{V}^3 = \eta_t + \eta_x u + \eta_y v \ ,$$

and Eq. (A11) becomes

$$k\partial_\tau \left(\frac{\rho}{|J|}\right) + \partial_\xi \left(\frac{\rho U}{|J|}\right) + \partial_\eta \left(\frac{\rho V}{|J|}\right) = 0. \tag{A15}$$

Eqs. (A14) and (A15) are the desired equations and are used in Section II.

APPENDIX B

COMPUTATIONAL MESH

a) ξ — Direction Mesh Distribution

i	ξ	i	ξ	i	ξ
1	-.300000 E+02	51	-.500000 E+00	101	.500000 E+00
2	-.237062 E+02	52	-.480000 E+00	102	.520000 E+00
3	-.187520 E+02	53	-.460000 E+00	103	.540000 E+00
4	-.148554 E+02	54	-.440000 E+00	104	.560000 E+00
5	-.117937 E+02	55	-.420000 E+00	105	.580000 E+00
6	-.939063 E+01	56	-.400000 E+00	106	.600000 E+00
7	-.750718 E+01	57	-.380000 E+00	107	.620000 E+00
8	-.603333 E+01	58	-.360000 E+00	108	.640000 E+00
9	-.488218 E+01	59	-.340000 E+00	109	.660000 E+00
10	-.398506 E+01	60	-.320000 E+00	110	.680000 E+00
11	-.328770 E+01	61	-.300000 E+00	111	.700000 E+00
12	-.274720 E+01	62	-.280000 E+00	112	.720000 E+00
13	-.232969 E+01	63	-.260000 E+00	113	.740000 E+00
14	-.200837 E+01	64	-.240000 E+00	114	.760000 E+00
15	-.176209 E+01	65	-.220000 E+00	115	.780000 E+00
16	-.157411 E+01	66	-.200000 E+00	116	.800000 E+00
17	-.143122 E+01	67	-.180000 E+00	117	.820000 E+00
18	-.132297 E+01	68	-.160000 E+00	118	.840000 E+00
19	-.124112 E+01	69	-.140000 E+00	119	.860000 E+00
20	-.117913 E+01	70	-.120000 E+00	120	.880000 E+00
21	-.113186 E+01	71	-.100000 E+00	121	.900000 E+00
22	-.109522 E+01	72	-.800000 E-01	122	.920000 E+00
23	-.106601 E+01	73	-.600000 E-01	123	.940000 E+00
24	-.104167 E+01	74	-.400000 E-01	124	.960000 E+00
25	-.102020 E+01	75	-.200000 E-01	125	.980000 E+00
26	-.100000 E+01	76	0.	126	.100000 E+01
27	-.980000 E+00	77	.200000 E-01	127	.102020 E+01
28	-.960000 E+00	78	.400000 E-01	128	.104167 E+01
29	-.940000 E+00	79	.600000 E-01	129	.106601 E+01
30	-.920000 E+00	80	.800000 E-01	130	.109522 E+01
31	-.900000 E+00	81	.100000 E+00	131	.113186 E+01
32	-.880000 E+00	82	.120000 E+00	132	.117913 E+01
33	-.860000 E+00	83	.140000 E+00	133	.124112 E+01
34	-.840000 E+00	84	.160000 E+00	134	.132297 E+01
35	-.820000 E+00	85	.180000 E+00	135	.143122 E+01
36	-.800000 E+00	86	.200000 E+00	136	.157411 E+01
37	-.780000 E+00	87	.220000 E+00	137	.176209 E+01
38	-.760000 E+00	88	.240000 E+00	138	.200837 E+01
39	-.740000 E+00	89	.260000 E+00	139	.232969 E+01
40	-.720000 E+00	90	.280000 E+00	140	.274720 E+01
41	-.700000 E+00	91	.300000 E+00	141	.328770 E+01
42	-.680000 E+00	92	.320000 E+00	142	.398506 E+01
43	-.660000 E+00	93	.340000 E+00	143	.488218 E+01
44	-.640000 E+00	94	.360000 E+00	144	.603333 E+01
45	-.620000 E+00	95	.380000 E+00	145	.750718 E+01
46	-.600000 E+00	96	.400001 E+00	146	.939063 E+01
47	-.580000 E+00	97	.420000 E+00	147	.117937 E+02
48	-.560000 E+00	98	.440000 E+00	148	.148554 E+02
49	-.540000 E+00	99	.460000 E+00	149	.187520 E+02
50	-.520000 E+00	100	.480000 E+00	150	.237062 E+02
				151	.300000 E+02

b) η — Direction Mesh Distribution

$\eta = y - S(x,t)$

j	y
1	-.283650 E-14
2	.188308 E-01
3	.412027 E-01
4	.677793 E-01
5	.993481 E-01
6	.136843 E+00
7	.181370 E+00
8	.234240 E+00
9	.297005 E+00
10	.371501 E+00
11	.459898 E+00
12	.564756 E+00
13	.689097 E+00
14	.836476 E+00
15	.101107 E+01
16	.121779 E+01
17	.146236 E+01
18	.175148 E+01
19	.209290 E+01
20	.249562 E+01
21	.296999 E+01
22	.352782 E+01
23	.418255 E+01
24	.494926 E+01
25	.584473 E+01
26	.688734 E+01
27	.809692 E+01
28	.949432 E+01
29	.111010 E+02
30	.129379 E+02
31	.150249 E+02
32	.173791 E+02
33	.200129 E+02
34	.229332 E+02
35	.261386 E+02
36	.296182 E+02
37	.333506 E+02
38	.373030 E+02
39	.414318 E+02
40	.456841 E+02
41	.500000 E+02

APPENDIX C

EFFECTS OF VARIOUS APPROXIMATIONS TO FULL POTENTIAL THEORY ON PRESSURE COEFFICIENTS

We have made additional computations of the flow field about a thickening and subsequently thinning airfoil. These computations use two modifications to full potential theory which are intermediate in going to the complete approximations made by low frequency, small disturbance, transonic theory. The results of the two modifications are shown in Figures 8 and 9 for two different times of the flow.

The modification 1 results were obtained by replacing the actual airfoil shape boundary $y = S(x,t)$ by the line segment $y = 0$, for $0 \le x \le 1$. On that line segment, the airfoil boundary condition, Eq. (42) was replaced by the equation,

$$\phi_y = S_t + S_x \phi_x \quad . \tag{C1}$$

Modification 2 made the following assumptions. It also replaced the airfoil shape by the line segment $y = 0$. The airfoil boundary condition here became

$$\phi_y = S_t + S_x \quad . \tag{C2}$$

Also the formula for Cp, Eq. (16), was replaced by the low frequency, small disturbance, transonic formula

$$Cp = -2 (\phi_x - 1) ;$$

here ϕ_x is the full potential and not the perturbation potential. Both modifications used the full potential equation, Eq. (18), as the governing equation.

In Figure 8, we see that both modifications give shock locations in good agreement with full potential theory. However Modification 2, with its small disturbance boundary conditions, yields the least expansion upstream of this shock and the weakest shock. In those two aspects, the intermediate theory, Modification 2, has less agreement with full potential theory than complete small disturbance theory has. Modification 1 only lacks the physical displacement of the fluid caused by the thickness of the airfoil. Modification 1 has good agreement with full potential theory, although on the first 60% of the airfoil Modification 1 gives slightly more negative values of Cp.

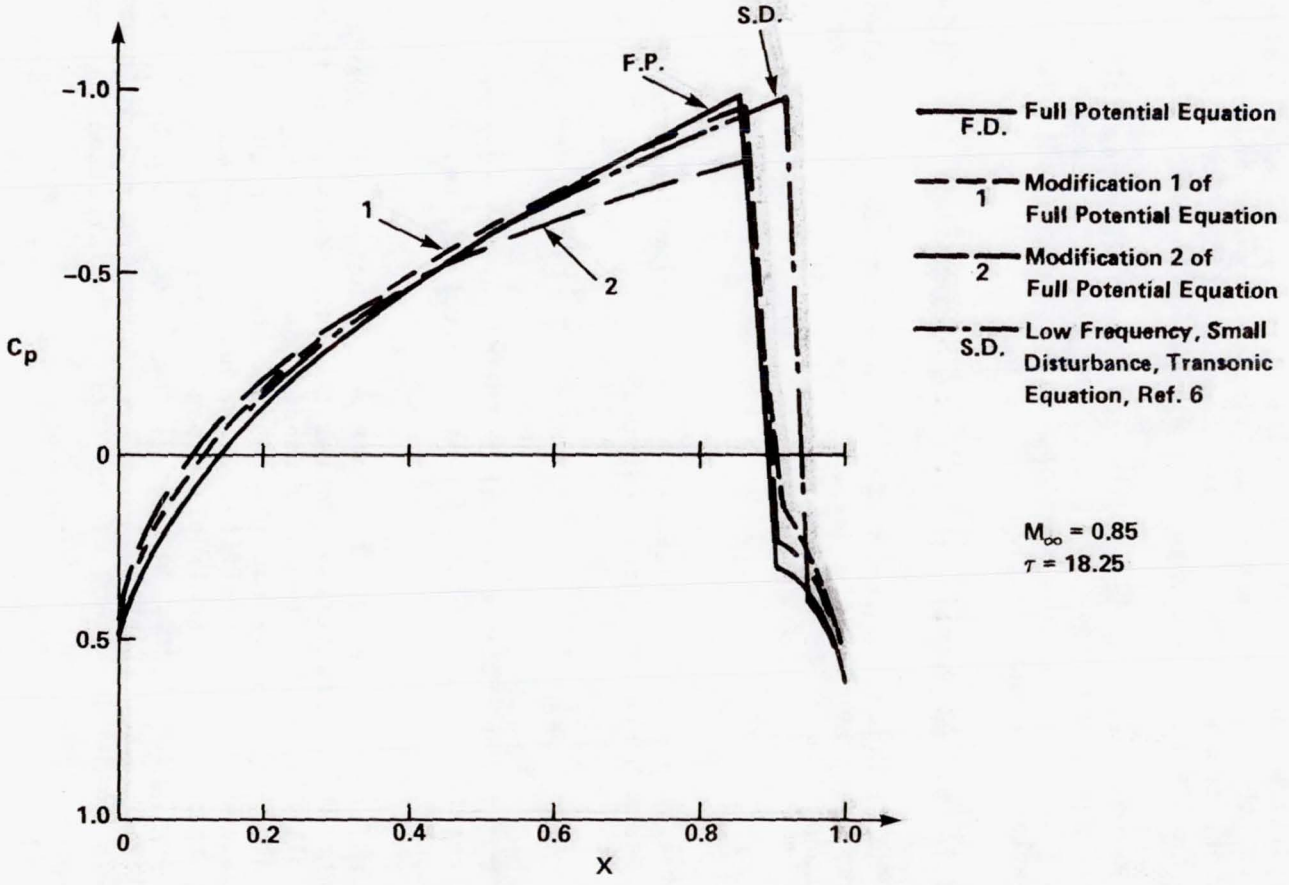

Figure 8.— Plot of Pressure Coefficients for Various Approximations to Full Potential Theory. Strong Shock Case.

In Figure 9, the modifications are plotted at a later time when the shocks are now weak. Again, Modification 1 is in close agreement with full potential theory; now the airfoil has almost no thickness. Modification 2 again has less agreement with full potential theory in the shock region than the complete small disturbance approximation has.

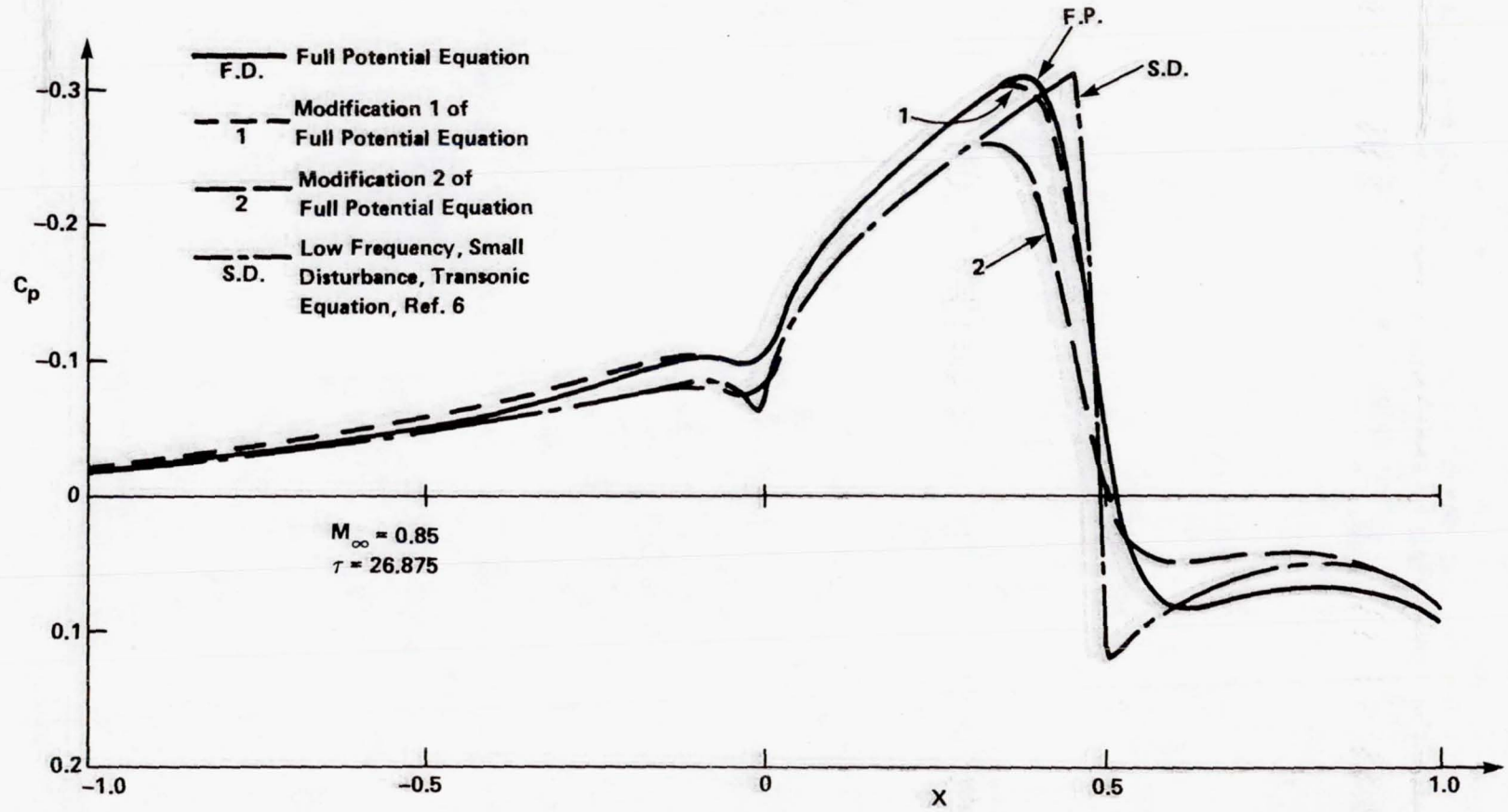

Figure 9.— Plot of Pressure Coefficients for Various Approximations to Full Potential Theory. Weak Shock Case.

REFERENCES

1. Davis, S. S. and Malcolm, G. N.: Experiments in Unsteady Transonic Flow. AIAA Paper 79-0769, April 1979.

2. Ashley, H.: On the Role of Shocks in the "Sub-Transonic" Flutter Phenomenon. AIAA Paper 79-0765, April 1979.

3. Isogai, K.: Calculation of Unsteady Transonic Flows Over Oscillating Airfoils Using the Full Potential Equation. AIAA Paper 77-448, March 1977.

4. Farmer, G. M. and Hanson, W. P.: Comparison of Supercritical and Conventional Wing Flutter Characteristics. Proceedings AIAA/ASME/SAE 17th Structures, Structural Dynamics and Materials Conf., King of Prussia, PA, April 1976, pp. 608-611. (See also NASA TM X-72837, May 1976.)

5. Caradonna, F. X. and Isom, M. P.: Numerical Calculation of Unsteady Transonic Potential Flow Over Helicopter Rotor Blades. AIAA Paper 75-168, January 1975.

6. Ballhaus, W. F. and Steger, J. L.: Implicit Approximate — Factorization Schemes for the Low-Frequency Transonic Equation. NASA TM X-73,082, November 1975.

7. Ballhaus, W. F. and Goorjian, P. M.: Implicit Finite — Difference Computations of Unsteady Transonic Flows about Airfoils. AIAA Journal, Vol. 15, December 1977.

8. Ballhaus, W. F. and Goorjian, P. M.: Computation of Unsteady Transonic Flows by the Indicial Method. AIAA Journal, Vol. 16, February 1978.

9. Warming, R. F. and Beam, R. M.: On the Construction and Application of Implicit Factored Schemes for Conservation Laws. SIAM-AMS Proceedings, Vol. 11, April 1977.

10. Beam, R. M. and Warming, R. F.: An Implicit Finite — Difference Algorithm for Hyperbolic Systems in Conservation Law Form. Journal of Computational Physics, Vol. 22, September 1976.

11. Houwenk, R. and van der Vooren, J.: Results of an Improved Version of LTRAN2 for Computing Unsteady Airloads on Airfoils Oscillating in Transonic Flow, AIAA Paper 79-1553, July 1979.

12. Pulliam, J. H. and Steger, J. L.: On Implicit Finite — Difference Simulations of Three Dimensional Flow. AIAA Paper 78-10, January 1978.

13. Steger, J. L.: Coefficient Matrices for Implicit Finite Difference Solution of the Inviscid Fluid Conservation Law Equations. Computer Methods in Applied Mechanics and Engineering, Vol. 13, 1978.

14. Ferrari, C. and Tricomi, F. G.: Transonic Aerodynamics, Academic Press, New York, 1968.

15. Lax, P. D.: Weak Solutions of Nonlinear Hyperbolic Equations and Their Numerical Computation. Communications on Pure and Applied Mathematics, Vol. 7, 1954, pp. 159-193.

16. Coburn, N.: Vector and Tensor Analysis, MacMillan, 1960.

17. Holst, T. L.: An Implicit Algorithm for the Conservative, Transonic Full Potential Equation Using an Arbitrary Mesh, AIAA Paper 78-1113, July 1978.

18. Jameson, A.: Transonic Potential Flow Calculations Using Conservative Form. AIAA Second Computation Fluid Dynamics Conf. Proc., June 1975, pp. 148-155.

19. Holst, T. L. and Ballhaus, W. F.: Fast, Conservative Schemes for the Full Potential Equation Applied to Transonic Flows. AIAA Journal, Vol. 17, February 1979.

20. Hafez, M. M. and Murman, E. M.: Artificial Compressibility Methods for Numerical Solution of Transonic Full Potential Equation. AIAA Paper 78-1148, July 1978.

21. Ames, W. F.: Numerical Methods for Partial Differential Equations. Academic Press, New York, 1977.

22. Ballhaus, W. F.: Some Recent Progress in Transonic Flow Computations. Von Karman Institute for Fluid Dynamics, Lecture Series 87, Computational Fluid Dynamics, Rhode-St.-Terese, Belgium, March 1976.

23. Beam, R. M. and Ballhaus, W. F.: Numerical Integration of the Small-Disturbance Potential and Euler Equations for Unsteady Transonic Flow. NASA SP-347, Vol. 2, March 1975.

24. Ballhaus, W. F., Magnus, R., and Yoshihara, H.: Some Examples of Unsteady Transonic Flows Over Airfoils. Proceedings of the Symposium on Unsteady Aerodynamics, Vol. II, pp. 769-791, University of Arizona, 1975.

25. Ballhaus, W. F., Holst, T. L., and Steger, J. L.: Implicit Finite — Difference Simulations of Steady and Unsteady Transonic Flows. Sixth International Conference on Numerical Methods in Fluid Dynamics, Tbilisi, USSR, June 1978, to be published in Lecture Notes in Physics, Springer Verlag.

26. Schouten, J. A.: Tensor Analysis for Physicists, Oxford, 1951.

27. Lass, H.: Vector and Tensor Analysis, McGraw-Hill, 1950.

28. Adler, R., Bazin, M., and Schiffer, M.: Introduction to General Relativity, McGraw-Hill, 1965.